Landau spectra of ZnH and neutral Zn in germanium

Keiichi Ishida
University of Wollongong

Landau Spectra of ZnH and Neutral Zn in Germanium

A thesis submitted in fulfillment of the

requirements for the award of the degree

Master of Science (Physics)

from

University of Wollongong

by

Keiichi Ishida

School of Engineering Physics

2004

Abstract

Far-infrared absorption spectroscopy was carried out on samples of germanium cut from single-crystal ingots doped with zinc. The ingots were grown in a hydrogen atmosphere and hence also contained the axial complex ZnH. Landau studies were made in the Voigt configuration for both the acceptors neutral zinc, Zn^0, and ZnH with **B** oriented along <100> crystallographic directions. Measurements were made in a super-conducting magnet with field strengths up to 6 T for both ZnH and Zn^0 using a modified slow-scan Polytec FTIR spectrometer. The incident radiation was plane polarised either parallel or perpendicular to the field. It was found that the main Landau features for both acceptors are the same as for the group III single-hole acceptor boron. The difference is in the fine-structure of the Landau lines which reflects the different natures of the acceptors boron, Zn^0 and ZnH.

Acknowledgments

I would like to thank both my supervisors, Professor Peter Fisher and Dr. Rodney E.M. Vickers for their guidance and encouragement.

I would like to thank the following people for their assistance:

Members of the Engineering Physics Department technical staff, especially Peter Anthony, Peter Ihnat and John Bourke.

Members of the Engineering Physics Department; academic and general staff.

Purdue University for supplying the samples.

Finally, I give special thanks to my family and friends for their support and encouragement.

Contents

List of Figures

List of Tables

Chapter 1. Introduction

In 1930, de Haas and van Alphen [1] observed that the magnetic susceptibility of bismuth exhibited an oscillatory behaviour with changing magnetic field strength and different crystallographic orientations. In the same year Shubnikov and de Haas [2] reported a similar result associated with the electrical conductivity of the same material. Without knowing of the de Haas-van Alphen effect (dHvA), Landau [3] developed his theory of the diamagnetism of a free electron gas. He demonstrated that in a uniform magnetic field, **B**, the energy states of such electrons in their classical circular motion in the planes perpendicular to **B** were condensed into a series of equally-spaced, parabolic bands, giving a quantisation of the closed magnetic orbits of the electrons. The density of these states was essentially localised at the bottom of each band to give a very narrow, energy-wise, distribution of the electrons. This set of magnetic subbands have become known as ***Landau levels*** and strongly influence the magnetic properties of metals and semiconductors and their behaviour as a function of B (=|**B**|). Thus Landau *predicted* the dHvA effect. Both of these effects have been exploited extensively for probing the nature of the Fermi surfaces in solids. A history of the dHvA effect and its uses has been given by Shoenberg[4]. These and other oscillatory effects have been described by Kahn and Frederikse [5].

Another experimental technique based on the formation of Landau levels is that of cyclotron resonance. This phenomenon, classically, is the result of electromagnetic radiation being absorbed when its frequency matches that of the frequency of the electrons in their closed orbits; the latter frequency is that of an electron in a cyclotron, ω_c, and is given by B/em_e, where m_e is the inertial mass of the electron. Quantum mechanically, the resonance corresponds to transitions of electrons from one Landau level to the next higher, these being separated by $\eta\omega_c$ (see Chapter 2). This process provides a means to measure the mass of the electron which, in solids, is not necessarily the inertial mass; it is usually designated as the effective mass which conceals the periodic potential of the crystal. The sharpness of the observed resonances requires that the broadening of the Landau levels by scattering mechanisms is small which, classically, means that the particle executes several revolutions before being scattered out of its orbit. Early cyclotron resonance experiments involved silicon and germanium [6 ,7] and measured in detail the anisotropy of the effective masses of the electrons at the bottom of the conduction bands and the holes at the top of the valence bands.

Cyclotron resonance was next reported for metals using the experimental procedure developed by Azbel' and Kaner [8].

The Landau levels also play a role in magneto-optical effects. For example, the optical absorption spectrum at and near the absorption edge of a semiconductor exhibits oscillations due to transition of electrons from the valence band Landau levels to those in the conduction band. Early observations of these were reported in the 1950's [9]. In addition, the photo-ionisation spectra of impurities in semiconductors under **B** contain oscillations due to transitions of electrons or holes from the ground states to the Coulomb-related Landau states. The first observation of these was for group V donors in germanium [10] while those for group III acceptors in this material were observed soon after [11]. Extensive measurements on the latter, particularly for boron, have been carried out by Takacs [12]. Recently, this technique has been extended to the study of neutral zinc, a double acceptor in germanium, and to axial acceptors in germanium [13]. It is the purpose of the present thesis to extend the previous studies of neutral zinc and the axial defect, ZnH, in germanium.

Chapter 2. Theoretical

The treatment of the behaviour of electrons in a magnetic field in both a constant and a periodic potential has developed through several stages. A few, pertinent to the problem at hand, will be mentioned. First, as introduced earlier, there was that of Landau [3]. Later there was the work of Luttinger and Kohn [14], and Luttinger [15]; they extended the effective mass theorem [16] to complex semiconductor structures in which the conduction band minima did not occur at $\mathbf{k} = 0$ and where the top of the valence band, although at the Brillouin zone centre, was degenerate. Both these situations exist for Si and Ge. Such calculations were particularly applicable in connection with cyclotron resonance and impurity states in semiconductors. The theory of Luttinger [15] was applied by Wallis and Bowlden [17] to give numerical results for the Landau levels of the valence band of Ge. Because of the complexity of the energy states, Suzuki and Hensel [18] and Hensel and Suzuki [19] recognised that the application of an external uniaxial force would lift the degeneracy at the top of the valence band and would simplify interpretation of the experimental results. They carried out both the theoretical and experimental work for this arrangement.

2.1 Landau States for Free Electrons

The total energy, ε, for an electron in a constant potential, V, is the same as the kinetic energy, T, if V is arbitrarily set to zero, *i.e.*, for a non-relativistic electron of momentum **p** and wave vector **k**

$$\varepsilon(\mathbf{k}) = T(\mathbf{k}) = \mathbf{p}.\mathbf{p}/2m_e = \eta^2\mathbf{k}.\mathbf{k}/2m_e = \eta^2(k_x^2 + k_y^2 + k_z^2)/2m_e, \quad (2.1)$$

where m_e is the inertial mass of the electron. Under an applied magnetic field **B** along the z-direction, the energy has been shown [3] to be

$$E_n = (s + 1/2)\eta\omega_c + \eta^2 k_z^2/2m_e;\ s = 0, 1, 2, 3,\ldots\ldots \quad (2.2)$$

This result is that obtained for the quantised states of a simple harmonic oscillator. The classical circular trajectories of the electron in the xy-plane can be resolved into two simple linear harmonic oscillators with angular frequency ω_c quantised as shown in Eqn (2.2), while p_z is unchanged.

The density of states for a three-dimensional free electron gas with **B** = 0 is given by

$$g_0(\varepsilon) \propto 2A\sqrt{\varepsilon}, \qquad (2.3)$$

while, for such gas in a uniform **B**, it is

$$g_L(\varepsilon) = A\frac{\hbar\omega_c}{\sqrt{[\varepsilon - (n + 1/2)\hbar\omega_c]}}, \qquad (2.4)$$

where $A = \frac{1}{4\pi^2}(\frac{2m_e}{\hbar^2})^{3/2}$. The results of Eqns (2.1) – (2.4) are shown in Figure 2.1. Note that the plots of $g_L(\varepsilon)$ are for individual values of n. It is thus seen, as mentioned in the Introduction, that the electrons in the plane perpendicular to **B** are concentrated at the bottom of each sub-band, *i.e.*, at $k_Z \approx 0$, hence the origin of the term Landau level.

2.2 Landau States for Electrons in Semiconductors

The application of the effective mass theory to the cases of Si and Ge was carried out by Luttinger and Kohn [14]. In this theory, a mass tensor replaces the effect of the periodic potential of the crystal, the elements of which are determined by the unperturbed band structure. They show that, if the spin-orbit coupling is neglected, the energy levels of an electron at the top of the valence band in a magnetic field **B** are given by

$$\sum_{j'}[D_{jj'}^{\alpha\beta}(p_\alpha + eA_\alpha)(p_\beta + eA_\beta)]F_{j'}(\mathbf{r}) = EF_j(\mathbf{r}). \qquad (2.5)$$

Here j runs over the number of degenerate states at the band edge, while α and β are dummy suffixes and are summed over x, y and z; $p_\alpha = \frac{1}{i}\frac{\partial}{\partial x_\alpha}$ and the Landau gauge is chosen for **A**, the magnetic vector potential. Also

$$D_{jj'}^{\alpha\beta} = \frac{1}{2m}\delta_{jj'}\delta_{\alpha\beta} + \frac{1}{m^2}\sum_i \frac{p_{ji}^{\alpha}p_{ij}^{\beta}}{\varepsilon_0 - \varepsilon_i}. \qquad (2.6)$$

Here the summation over i includes all those states of the unperturbed crystal other than the set j, ε_0 is the energy of the degenerate set while ε_i is the energy of the i^{th} unperturbed state. The wave function of the system is given by

$$\psi = \sum_j F_j(\mathbf{r})\phi_j \qquad (2.7)$$

where the ϕ_j are the degenerate Bloch functions of the unperturbed crystal.

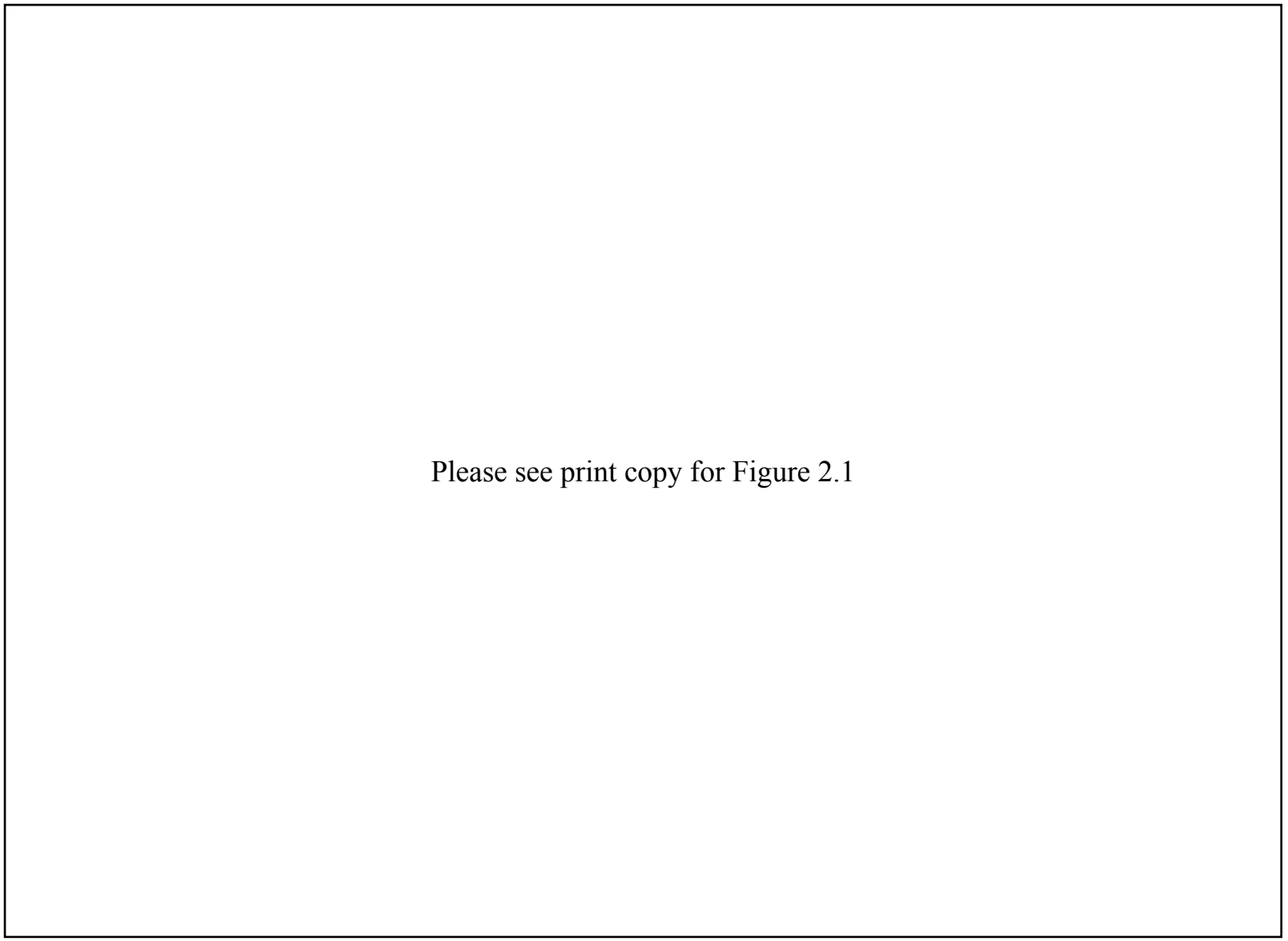

Fig. 2.1. Results of Landau's treatment [3] of the behaviour of free electrons in a homogeneous magnetic field.

If a matrix is defined by $D = \left[D_{jj'}\right] = \left[D_{jj'}^{\alpha\beta} k_\alpha k_\beta\right]$ for the diamond structure at **k** = 0, without spin-orbit coupling and **B** = 0, assuming that the cubic axes of the crystal coincide with the coordinate axes, we have,

$$D = \begin{vmatrix} Ak_x^2 + B(k_y^2 + k_z^2) & Ck_xk_y & Ck_xk_z \\ Ck_xk_Y & Ak_y^2 + B(k_z^2 + k_x^2) & Ck_yk_z \\ Ck_xk_z & Ck_yk_z & Ak_z^2 + B(k_x^2 + k_y^2) \end{vmatrix}, \qquad (2.8)$$

where A,B and C are real constants given by the appropriate $D_{jj'}^{\alpha\beta}$'s. Introduction of spin-orbit coupling lifts some of the degeneracy at **k** = 0 to give a four-fold degeneracy at the band edge separated from a band of two-fold degeneracy, the latter being of lower energy. The spin-orbit splitting of these bands is called λ.

Cyclotron resonance experiments involved electromagnetic energies small compared to λ □□□ thus the higher lying band could be treated separately. The resulting energy states are still described by the same set of constants A, B and C of the unperturbed bands. Luttinger and Kohn [14] did not solve the set of coupled differential equations to give the energies but recognise that for high quantum numbers these lead to equally spaced Landau levels but for low quantum numbers there are deviations from this.

The next stage of this development was due to Luttinger [15]. He pointed out that in the derivation of Eqn. 2.5 by Luttinger and Kohn [14] that it was assumed that $D_{jj'}^{\alpha\beta} = D_{jj'}^{\beta\alpha}$. He demonstrates that this is not true in general, whereas what is true is that $(D_{jj'}^{\alpha\beta})^* = D_{j'j}^{\beta\alpha}$. Introduction of the difference $D_{jj'}^{\alpha\beta}$ - $D_{jj'}^{\beta\alpha}$ requires a fourth constant, K, to be invoked when a magnetic field is present. When spin–orbit coupling is included with a magnetic field a fifth constant, designated by β_5, is required. Thus, a total of five constants is now needed to describe the energies of the Landau levels. He finds it convenient to use the five dimensionless constants, γ_1, γ_1, γ_1, κ and q, defined by

$$\frac{1}{2m}\gamma_1 = -\frac{1}{3}(A + 2B) \qquad \frac{1}{m}(3\kappa + 1) = -K$$

$$\frac{1}{2m}\gamma_2 = -\frac{1}{6}(A - B) \qquad \frac{e}{mc}q = -\beta_5\ ; \qquad (2.9)$$

$$\frac{1}{2m}\gamma_3 = -\frac{1}{6}C$$

these also give hole energy. These five constants are called Luttinger parameters. The values he quotes for the first three for Ge are 13.2, 4.4 and 5.4, respectively. In his discussion of the energy levels, Luttinger considers an approximation for Ge based on taking $\gamma_2 = \gamma_3 = (\gamma_2 + \gamma_3)/2$, $q = 0$ and $k_z = 0$ and then uses perturbation theory to incorporate $\gamma_3 - \gamma_2$ and a non-zero q. He does not give any numerical results or comparison with experiment but implies that the general prediction of quantum deviations in the Landau ladders are in agreement with the cyclotron resonance experiments of Fletcher, *et. al.*, [20]. There are four Landau ladders at **k** = 0; this is where the two two-fold degenerate bands coincide. Two ladders are associated with the "light holes" and two with the "heavy holes".

The next application of the Luttinger theory was by Wallis and Bowlden [17] who give numerical results for the Landau levels of the valence band of Ge. In these calculations, the Luttinger parameters, γ_2 and γ_3, are again taken to be equal to the mean value of the two, $q = 0$ and, initially, $k_z = 0$. A quantitative diagram is given of the four Landau ladders. He then extends the calculations to show the effect of a small but non-zero k_z.

Suzuki and Hensel [18] pointed out that advancement in this area was hampered by the extreme difficulty in identifying the cyclotron resonances because of the quantum deviations at the bottom of each ladder. The original results for Ge and Si [6, 7] were under experimental conditions which produced resonances higher up in the ladders where correspondence with the classical frequency prevailed. They also recognised that numerical computations to aid in the identification of the resonances were not reliable because the Luttinger parameters were not sufficiently precise. (A further problem was the neglect of k_z.) They resolved this situation by applying a uniaxial stress to the Ge samples, thus decoupling the degenerate valence band to give easy identification of the resonances and determine the Luttinger parameters with high precision. With this information and the inclusion of k_z they return to analysing the spectra of unstressed Ge. Their results for γ_1, γ_2, γ_3, κ and q were 13.38±0.02, 4.24±0.03, 5.69±0.02, 3.41 and 0.06, respectively [19]. This paper gives their calculated results for low-lying Landau levels at $k_z = 0$. This data is reproduced in Figure 2.2 for **B**||<100>, <111> and <110>.

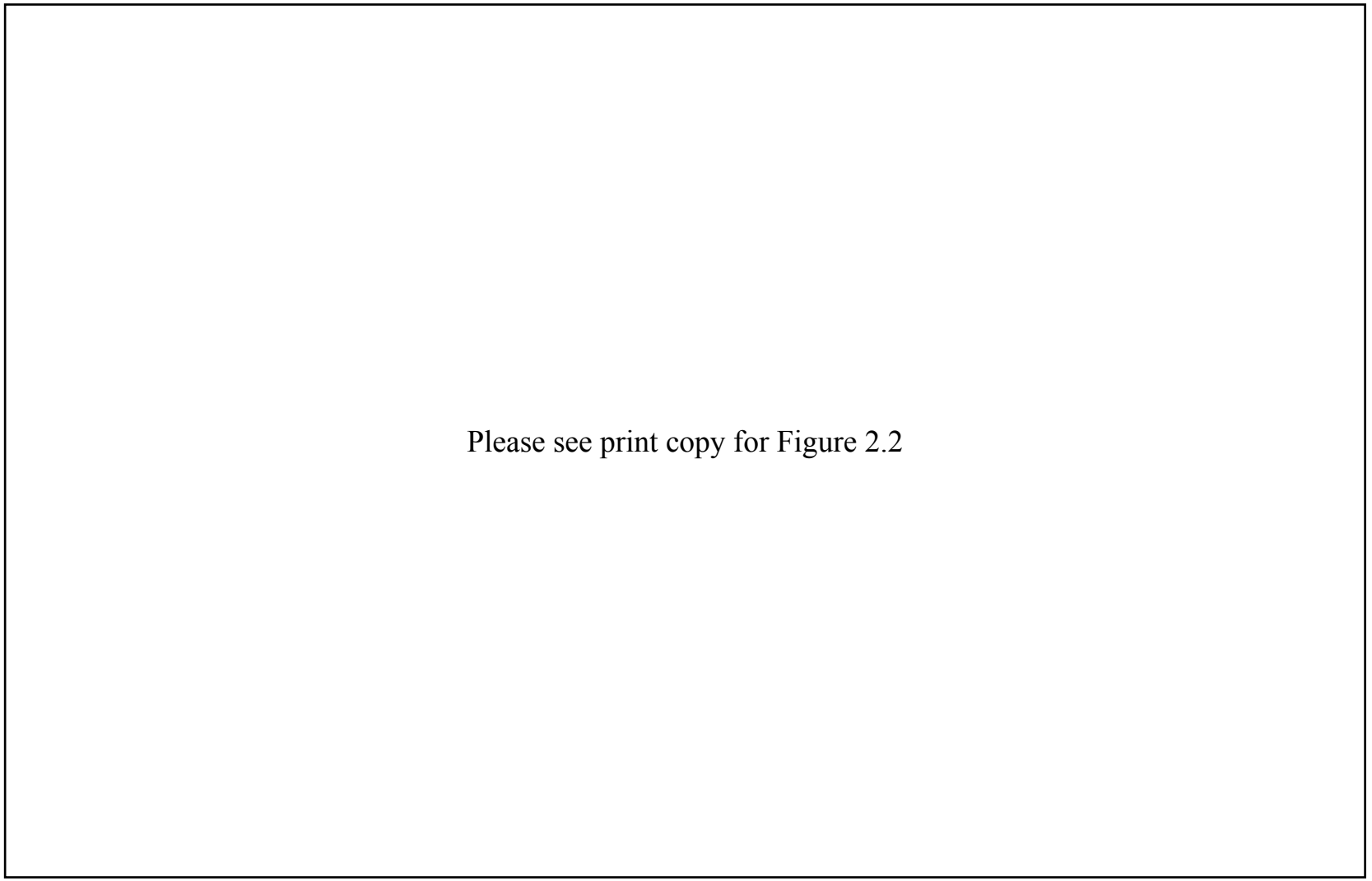

Fig. 2.2. Valence band Landau levels in germanium as calculated by Hensel and Suzuki [x].

The labels on the states in the four Landau ladders in Figure 2.2 have the following meaning. Suzuchi and Hensel [18] define an operator $\mathbf{N} = \mathbf{J_3} + \mathbf{a}^\dagger\mathbf{a} + 3/2$, where $\mathbf{J_3} = [\mathbf{J}_+, \mathbf{J}_-]$ and $\mathbf{a}^\dagger$ and $\mathbf{a}$ are the harmonic oscillator creation and annihilation operators, respectively, and $\mathbf{J}_+$ and $\mathbf{J}_-$ are the raising and lowering angular momentum operators, respectively, for J = 3/2. The eigenvalues of N are

$$N = M_J + n + 3/2. \qquad (2.10)$$

Since $M_J = \pm 1/2$ and $\pm 3/2$, then $N \geq n = 0, 1, 2, 3, 4, \ldots\ldots\ldots$ .The states are labelled as N_n, the value of n distinguishing the four states with the same N, the Landau quantum number. An additional label is given to each state, *viz*., V^π, where V = N(modulo ν) and π is the parity. Here ν is the foldedness of the rotational symmetry along the direction of **B**. Equation 2.10 shows that those levels with the same value of N – n have the same M_J, thus for N – n = 0, 1, 2 and 3, $M_J = -3/2, -1/2, +1/2$ and $+3/2$. It is interesting to note that in Figure 2.2 three of the ladders are characterised by a different but single value of M_J while the fourth, a light hole ladder, contains a mixture of $M_J = -1/2$ and $+3/2$.

It has been demonstrated [12] that the dominant Landau absorption lines due to acceptors in Ge are transitions from the ground states of the impurities to the Coulomb-related light hole Landau levels (LHLL) (see Section 2.3 below). The symmetries of the associated LHLL's have been determined [12] by application of an equation due to Suzuki and Hensel [18]. For the case of **B**||<100>, for example, this equation is

$$C_\nu \,|V\rangle = e^{-(2K-3)i\pi/\nu}\,|V\rangle, \qquad (2.11)$$

where the point group of the system is C_{4h} and thus $\nu = 4$. The symmetries of the LHLL have been tabulated by Takacs [12] and, for **B**||<100> at **k** = 0, are as follows:

$$V = 0: \quad 0_0, 4_1, 4_4, 8_5\ldots\ldots \; ; \; \Gamma_7^\pm \qquad (2.12a)$$

$$V = 1: \quad 1_0, 1_1, 5_2, 5_5,\ldots\ldots \; ; \; \Gamma_6^\pm \qquad (2.12b)$$

$$V = 2: \quad 2_1, 2_2, 6_3, 6_6,\ldots\ldots \; ; \; \Gamma_5^\pm \qquad (2.12c)$$

$$V = 3: \quad 3_0, 3_3, 7_4, 7_7,\ldots\ldots \; ; \; \Gamma_8^\pm. \qquad (2.12d)$$

Here the Γ's are the double group representations of C_{4h} (see, for example, Koster *et al.* [21]).

2.3 Landau States and Bound Hole States

The introduction of shallow acceptor impurities into a semiconductor produces bound hole states in the energy gap at $k_z = 0$ and close to the top of the valence band. The spectra of these, due to transitions between the bound states, have been studied extensively with and without external perturbations [12]. The impurity states are obtained from an adaptation of the effective mass theory to include the Coulomb potential of the charged acceptor into the Hamiltonian. It is the inclusion of these defects in the otherwise perfectly periodic crystal that allows the states to be in the normally "forbidden energy" gap. These states are constructed from those at the top of the valence band and the hydrogenic functions describing the motion of the hole bound to the charged impurity.

Application of a magnetic field produces the Landau sub-bands, each of which has Coulomb-related quasi-bound states associated with it. The transitions from the ground state of such acceptors to these Coulomb-related Landau states is to be studied here for two types of acceptors. The first observation of such spectra was for boron in Ge [11], while more recently a very extensive study of this has been carried out [12]. Identification of the Coulomb-related Landau excited states involved has relied heavily [12] on the predictions of Hensel and Suzuki shown in Figure 2.2, the predictions by Wallis and Bowlden [22] for a non-degenerate parabolic band at $\mathbf{k} = 0$ and Lin-Chung and B. W. Henvis [23] for non-parabolic, degenerate bands; both the latter compare their results with the experimental observations for donors in InSb. The aspect which arises from these results is the binding energies of these states relative to the bottom of their associated Landau level should increase with field.

2.4 Selection Rules for B||<100>

2.4.1 Zn–H in Ge

It is well known that Zn–H substitutional defects in Ge have their axes along the four <111> covalent bond directions [24, 25]; this reduces the point group symmetry from that of $T_d(O_h)$ to $C_{3v}(D_{3d})$. (The two notations given here reflect the way the

theory of bound acceptor states has developed. The O_h notation is that introduced by Baldereschi and Lipari [26] in their novel approach to the problem. The T_d point group notation describes the true symmetry of substitutional defects in Ge). Thus, without external perturbation the four-fold degenerate ground state, originally of symmetry $\Gamma_8(\Gamma_8^+)$ □□ $\bar{T}_d(\bar{O}_h)$, is split into two two-fold Kramers' doublets, $\Gamma_4(\Gamma_4^+)$ and $\Gamma_5(\Gamma_5^+)+\Gamma_6(\Gamma_6^+)$ of $\bar{C}_{3v}(\bar{D}_{3d})$. The latter two one-dimensional double group representations are complex conjugates of each other and their sum will be written as Γ_{5+6}^+. Here the parity label introduced by Baldereschi and Lipari [26] *via* their spherical approximation (and retained by them and others in subsequent calculations) has been included; this labelling will be used in what follows. Figure 2.3 shows these results and includes the case of a group III acceptor. Also shown is the effect of **B**||<100> on both types of acceptors. The internal splitting of the ground state of ZnH, defined as Δ_{int} in Figure 2.3, is known [24, 25] to be large enough that at liquid He temperatures the Γ_4^+ ground state is not occupied to any extent and thus observed transitions are only from the Γ_{5+6}^+ ground state. Under **B**||<100>, all four axial types of ZnH are effected to the same extent causing the ground state of each type to undergo the same Zeeman splitting; the new symmetry is C_i with each Zeeman state belonging to the same irreducible representation $\Gamma_2^{\pm}$ (see Figure 2.3). The selection rules for electric dipole transitions permit these from both Zeeman sub-states to all other states for **E**||**B** and **E**⊥**B**, where **E** is the electric field of the electromagnetic radiation. The splitting of the Γ_{5+6}^+ ground state with field has been determined previously [25]. Also shown in Figure 2.3 is the Zeeman splitting of the Γ_8^+ ground state of group three acceptors.

2.4.2 Neutral Zinc (Zn^0) in Ge

The symmetries of the ground states of double acceptors in Ge are given by the antisymmetric direct product $\{\{\Gamma_8^+ x \Gamma_8^+\} = \Gamma_1^+ + \Gamma_3^+ + \Gamma_5^+$ of $\bar{O}_h$; the orbitals of the two holes being each of symmetry Γ_8^+ [27]. It has been shown both experimentally [28, 29] and theoretically [30] that for Zn^0, the Γ_1^+ state is the lowest in energy and is the only

one significantly populated at liquid He temperatures. Thus all observed transitions for samples at these temperatures are from $1\Gamma_1^+$. It has been demonstrated that the observed

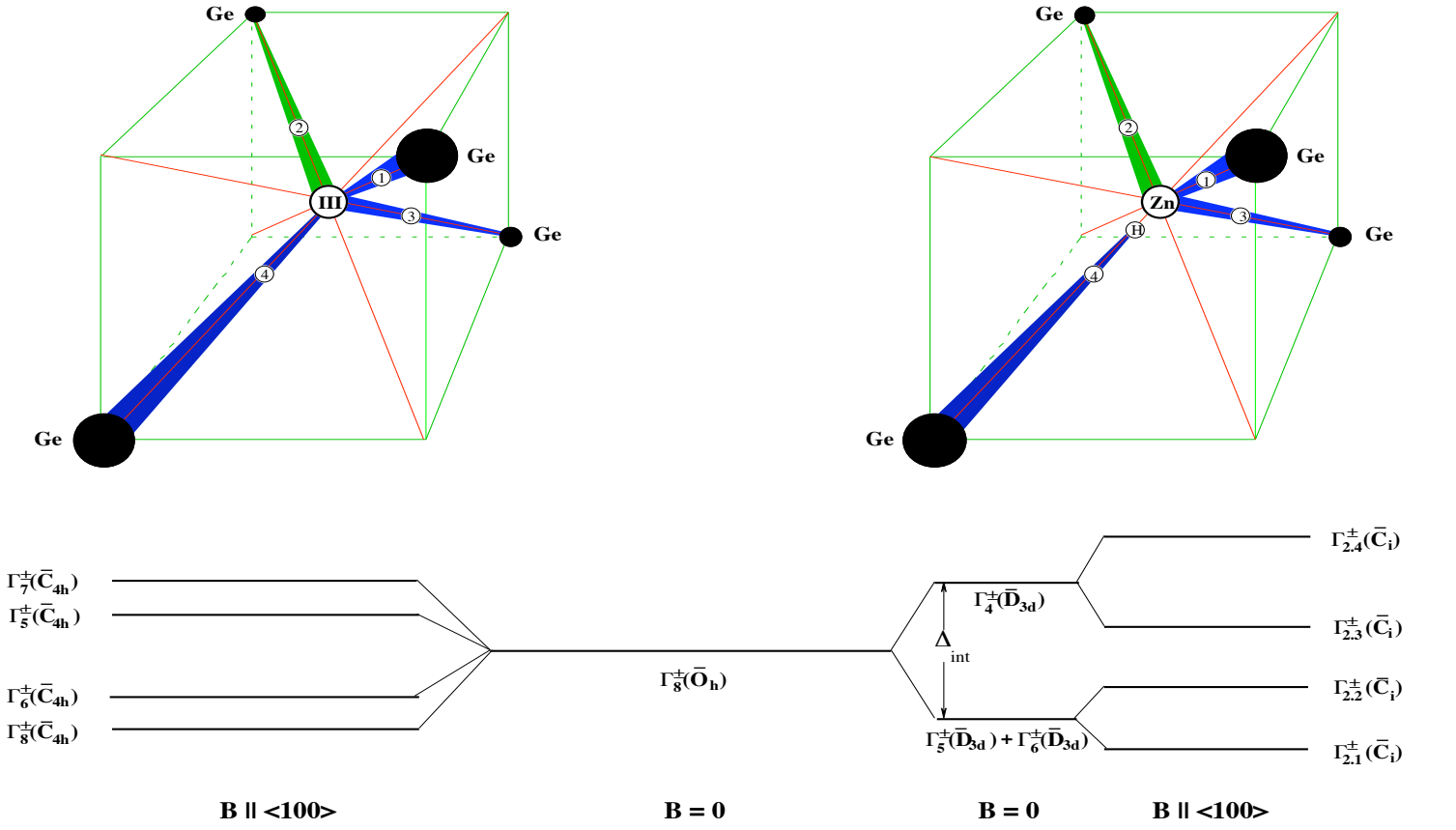

Fig. 2.3. Energy states of group III and axial defects in Ge for **B**||<100>.

optical absorption spectrum is due to the excitation of one of the holes to the various excited states. The orbital of the remaining hole becomes that of the hole in the ground state of singly ionised zinc, Zn^-; this has been shown to be true experimentally [29, 31]. Consequently, although the lowest ground state of Zn^0 is simple, its excited states are not. Their symmetry is given by the direct product of the symmetry of the orbital of the unexcited hole Γ^+_{uh} and that of the excited hole, Γ^-_{eh}, where for Zn^0, $\Gamma^+_{uh} = 1\Gamma^+_8(Zn^-)$. Under a magnetic field, $1\Gamma^+_8(Zn^-)$ splits into its four Zeeman states which, for **B**||<100>, are $1\Gamma^+_5$, $1\Gamma^+_6$, $1\Gamma^+_7$ and $1\Gamma^+_8$ all of $\bar{C}_{4h}$. This gives rise to four types of possible excited states for a given Γ^-_{eh}. The energy spacings of this quartet are just those of the Zeeman states of the J = 3/2 ground state of Zn^-. The magnitudes of these splittings are 0.25 cm^{-1}/T for the ±1/2 states and 0.75 cm^{-1}/T for the ±3/2 states [31]. The possible symmetries of Γ^-_{eh} for **B**||<100> are $1\Gamma^-_5$, $1\Gamma^-_6$, $1\Gamma^-_7$ and $1\Gamma^-_8$. Thus, the Landau transitions to be presented in this thesis will have excited states whose symmetries are $\Gamma^+_n x \Gamma^-_m$, where n, m = 5, 6, 7, 8 and Γ^-_m is the symmetry of the Coulomb states associated with a given Landau level. The selection rules for the transitions $1\Gamma^+_1 \rightarrow 1\Gamma^+_n x \Gamma^-_m$ are shown in Figure 2.4.

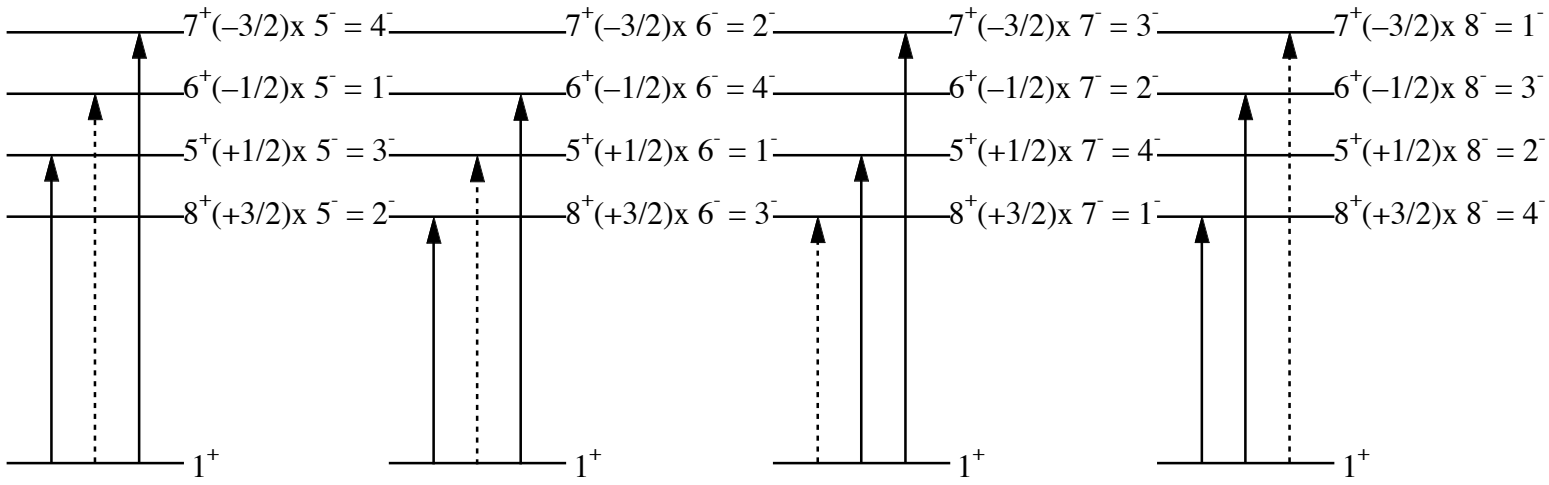

Fig. 2.4. Allowed Landau transitions for neutral zinc for **B**||<100>.
Straight line shows **E**⊥**B**, and dash line shows **E**||**B**.

Chapter 3. Experimental Techniques

3.1. Introduction

Fourier transform spectroscopy is based on the fact that an interferometer produces an interference pattern due to all the waves which enter it simultaneously thus giving a very high signal-to-noise ratio. Additionally, this signal-to-noise ratio can be enhanced by taking multiple scans, or by using a slow-scan speed with a matched electronic time constant. Measurements used in this thesis were made by either a Bomem fast-scan or a modified Polytec slow-scan spectrometer.

Most FTIR spectrometers are built based on the Michelson interferometer principle in which two beams of coherent radiation interfere to produce an interferogram. The radiation is collimated before being split into two beams by a beam splitter. One beam is reflected back to the beam splitter by a stationary mirror and the other one by a moving mirror; these are superposed to produce the interferogram. The interferogram will be a cosine wave if the source is monochromatic, and if polychromatic, it will be the sum of the cosines for each frequency. There will be a central maximum at zero optical path difference where all the cosines added constructively. By placing the material of interest in the combined beam after it leaves the interferometer modulation in the interferogram will be produced by any absorption of the radiation in the material. A Fourier transform is executed on the interferogram to obtain the transmitted spectrum.

The spectrum and the interferogram may be expressed as

Interferogram $$I(\delta) = \int_{-\infty}^{\infty} B(\sigma) e^{2\pi i \sigma \delta} d\sigma \qquad (3.1)$$

Spectrum $$B(\sigma) = \int_{-\infty}^{\infty} I(\delta) e^{-2\pi i \sigma \delta} d\sigma, \qquad (3.2)$$

where σ = frequency

δ = retardation = 2vt

v = mirror travel speed

t = time, set at zero at zero path difference

The transmitted spectrum may be acquired by executing an inverse cosine Fourier transform on I(δ)

$$B(\sigma) = \int_{-\infty}^{\infty} I(\delta)\cos(2\pi\sigma\delta)\, d\sigma \qquad (3.3)$$

which, if the function is even, is

$$B(\sigma) = 2\int_{0}^{\infty} I(\delta)\cos(2\pi\sigma\delta)\, d\sigma \qquad (3.4)$$

When measuring, the interferogram is sampled at a constant rate over a finite mirror travel, thus the interferogram will be that of a truncated cosine function of which the transform is a sinc function. The maximum theoretical unapodised resolution, $\Delta\bar{\nu}_{ua}$, associated with this mirror travel is $\Delta\bar{\nu}_{ua} = 0.74/\Delta_{max}$, where Δ_{max} is the maximum optical path difference between the two beams; the latter is twice the maximum distance travelled by the moving mirror. This expression is based on the criterion that the sum of two equally intense spectral lines (two identical sinc functions) separated by $\Delta\bar{\nu}_{ua}$, will have a dip of 20% of the total intensity of each peak at a point half-way between them.

3.2. Polytec FTIR 25 Spectrometer

A diagram of the modified Polytec FTIR 25 spectrometer is shown in Fig.3.1. The three main chambers are kept evacuated to remove atmospheric water vapour. In the chamber on the top of right, the radiation produced by the globar source is amplitude modulated with a mechanical chopper; this also controls the reference signal for synchronous detection. The chopped radiation is collimated by the off-axis paraboloidal mirror ahead of entering the interferometer. Several mylar beam splitters were used to cover the specific range required. The mirror displacement is measured by a rotary encoder, and there is a maximum displacement of 100 mm which limits the maximum unapodised resolution of the spectrometer to 0.037 cm^{-1}. The beam splitter in the FTIR 25 was at 30^{o} to the incident beam, as the Brewster angle for the mylar beam splitter is ~57°. This reduced polarisation due to reflections from the beam splitter surface. The ratio of vertical (**E**⊥**B**) to horizontal (**E**||**B**) polarisations is 1.7:1, where **E** is the electric vector of the radiation. After leaving the interferometer, the beam is focussed to pass though a wire grid polariser (consisting of gold evaporated onto a polyethylene replica grating as substrate) before falling on the sample mounted in the Voigt configuration between the split coils of an Oxford Instruments superconducting (SC) magnet.

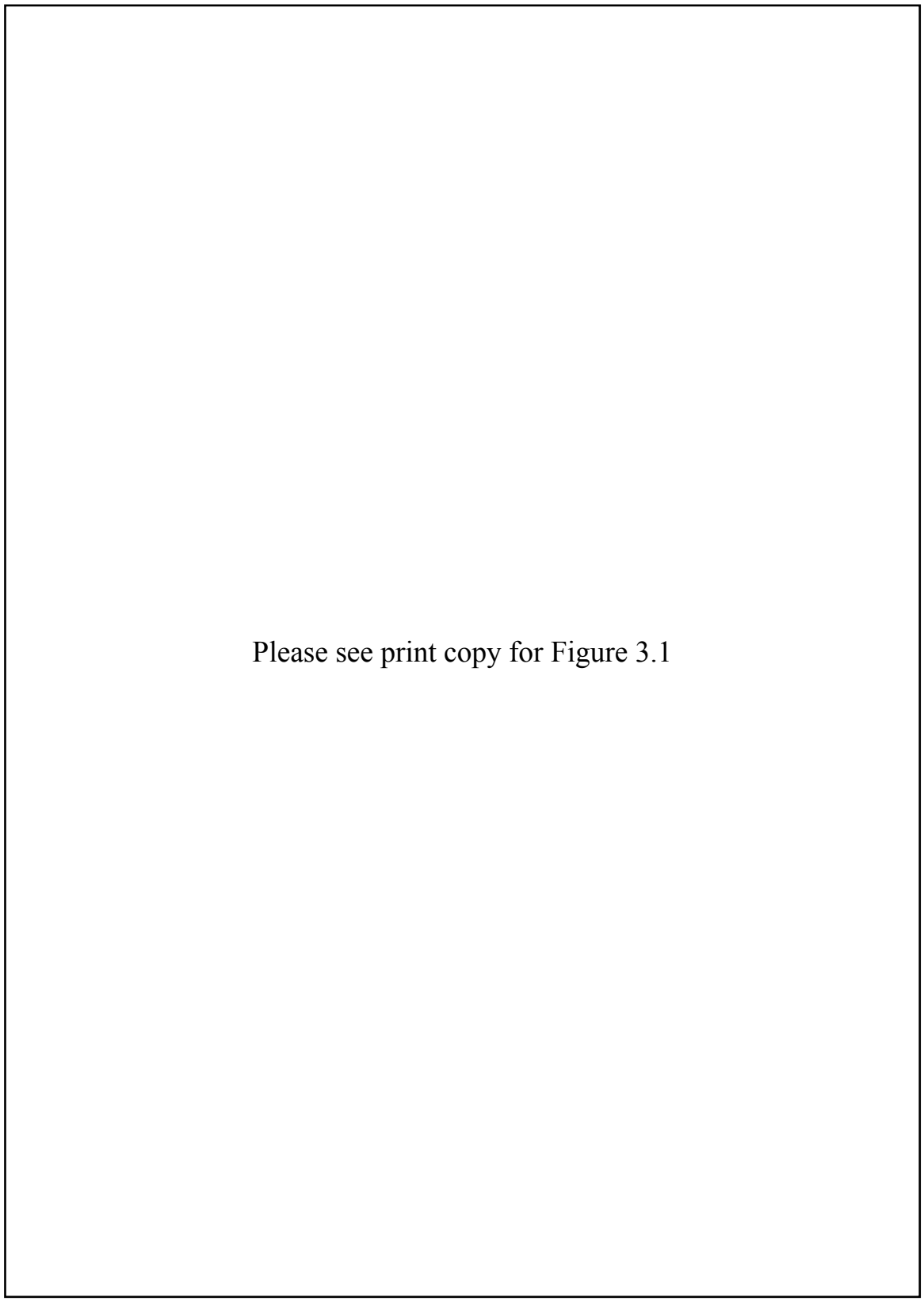
Please see print copy for Figure 3.1

Both the liquid helium and room temperature windows were polypropylene. The room temperature entrance window was an 0.8 mm thick disc with a cone machined into it, reducing the thickness to 0.4 mm at the apex to eliminate Edser-Butler fringes. The three other windows were unwedged and 50 μm thick. The sample was cooled to liquid helium temperature by syphoning He into the sample chamber of the magnet through a needle valve. The detector was an Infrared Laboratories (IRL) silicon bolometer whose output was connected to a PAR model 5209 lock-in amplifier. The cold filters of the bolometer detector determined the spectral regions; these were 10-110 cm^{-1}, 10-370 cm^{-1} and 50-700 cm^{-1}. The output from this amplifier was converted in a 16 bit analogue to digital converter before being recorded as an interferogram by a computer. The angular position of the sample about the vertical axis was measured by a laser mounted on the top of the sample stick.

3.3. Bomem FTIR Spectrometer

The Bomem spectrometer is a fast-scan interferometer producing a sinusoidal intensity variation of the beam with a specific frequency for each spectral element. This is amplified by a broad-band amplifer. The mylar beam splitter of this instrument is coated to cover the spectral range 10-700 cm^{-1}; either a globar or a mercury lamp was used as a source.

A schematic of the Bomem FTIR is showed in Figure 3.2. An off-axis ellipsoidal mirror located in the source chamber focuses the radiation onto an adjustable mechanical iris. After divergence the beam is collimated and made incident on the beam splitter to produce two beams. One beam goes to a stationary mirror directly, the other to a moveable mirror. These two beams return to the beam splitter and are superimposed, and the interfering collimated beams being refocused to a 1:1 image of the iris. The sample to be studied is located at this image. The beam through the sample is collected by a silicon bolometer through a light pipe. The cold filters in this detector are the same as above. The sample cryostat consist of stainless steel with a He reservoir into which the sample could be immersed. It could also be pumped to cool the sample below 4.2 K. The signal from the detector was fed to a high speed vector processor where a filter function was automatically generated for a particular spectral range and so reject the unwanted frequencies by numerical filtering.

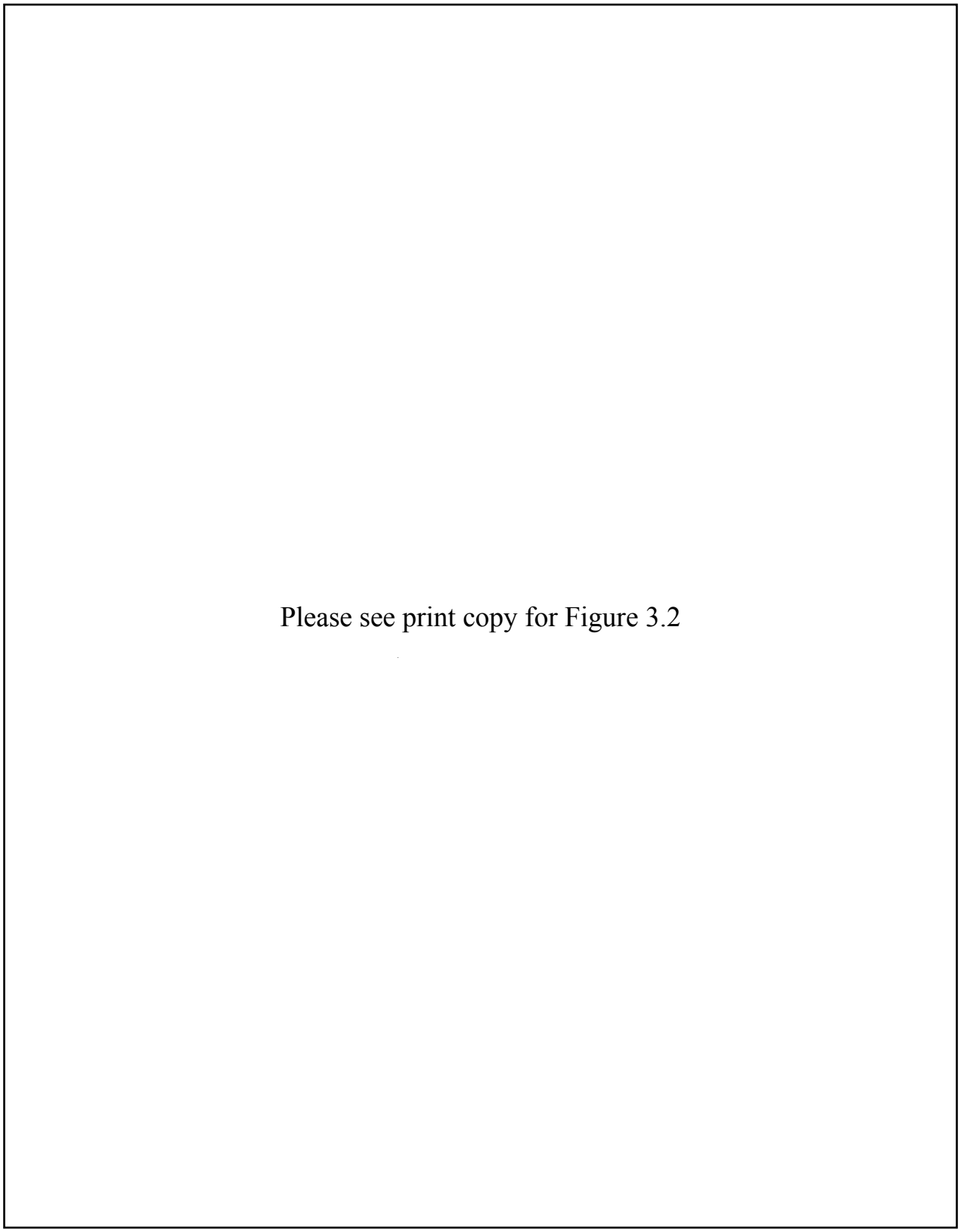

Figure 3.2. Schematic of Bomem FTIR spectrometer.

3.4. Sample Preparation

The samples used throughout this thesis were germanium single crystals doped with zinc and Zn-H; these were grown using the Czochalski method at Purdue University. The hall coefficients and resistivities were not measured. The hydrogen was introduced when the Zn doped ingots were grown and as a result it produces the axial complex Zn-H. The hydrogen gas was used as the ambient atmosphere for reduction purpose. Initially, each sample was roughly cut from an ingot using a wire saw with a glycerine-carborundum slurry; their widths were oriented along <100> directions. Next, the samples were ground with 1000 grit silicon carbide powder to erase saw marks and followed by 9μ and 1μ alumina powder for polishing. During grinding, the samples were wedged along their lengths to prevent Edser-Bulter fringes. In order to maximise the transmission of the samples in the spectral range of interest, several different surface treatments were used. The results of these tests are shown in Figure 3.3, the spectra being obtained using the Bomem instrument. The sample used here was first polished as above and its spectrum recorded. Following this it was etched in H_2O_2 (30%) at 85^o C for 6 mins. and the spectrum again recorded. After this it was again polished as before and the spectrum observed. The final treatment was to immerse it in water in a 43 KHz ultrasonic bath for 44 hrs (UST); this was to ensure that any bulk stress arising from the grinding and polishing of the sample was removed [32]. The spectrum was again taken. As can be seen from Figure 3.3, the transmission in the range between the ZnH and Zn^0 spectra, where Landau lines for ZnH should occur, is essentially the same for the upper two spectra. Thus, the Landau features of this defect were studied after the sample had been treated in the above sequence. For the sample used to study the Landau lines of Zn^0, only the sequence polish – etch – polish was used, it being assumed that the Lyman lines of the Zn^0 spectrum were sufficiently broad not to warrant the UST.

The intensity of radiation absorbed by, or reflected from, the sample is determined by the combination of two optical constants. One is the refractive index, n, and the other one is the extinction coefficient, k. Assuming a perfect surface, the reflectivity, R, can be calculated from

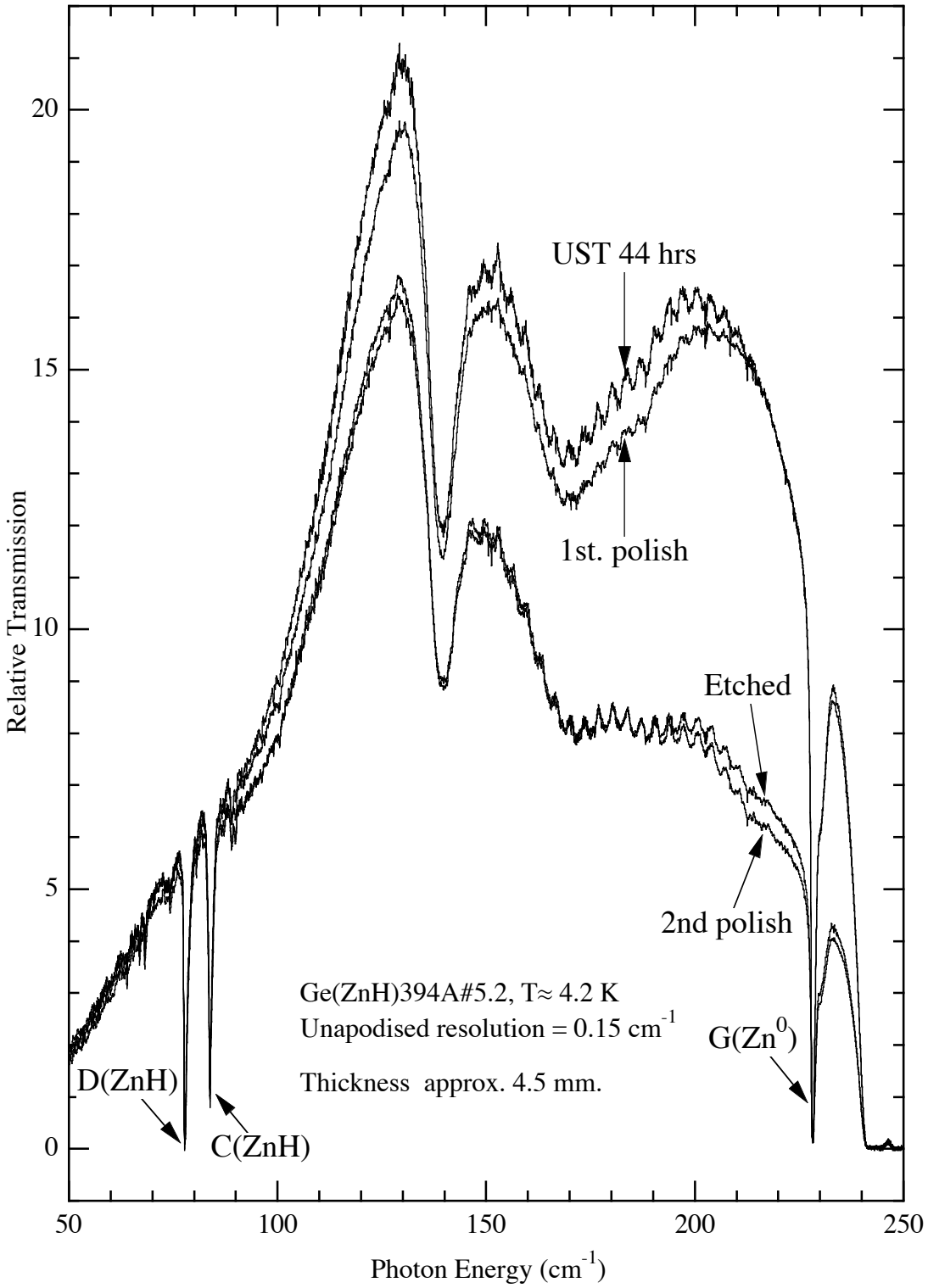

Fig. 3.3. The effect of different surface treatments for Ge(ZnH)394A#5.2.

$$R = \frac{(n-1)^2 + k^2}{(n+1)^2 + k^2} \tag{3.5}$$

The transmission, T, can be written as

$$T = \frac{I}{I_0} \approx \frac{(1-R)^2 e^{-\alpha x}}{1 - R^2 e^{-2\alpha x}}, \tag{3.6}$$

where I = transmitted intensity

I_0 = incident intensity

x = sample thickness

α = absorption coefficient $= \frac{4\pi k}{\lambda}$

λ = wavelength of incident radiation;

the approximation ignores the interference term since the sample is wedged. Inverse Fourier transforms were performed on the interferograms to obtain the spectra. These spectra were ratioed with I_0 to obtain the transmission spectra. The I_0 was measured by removing the sample from the beam. The absorption spectra were obtained by calculating the following inversion of Eqn. 3.6.

$$\alpha = -\frac{1}{x} \ln\left[\frac{-(1-R)^2 + \sqrt{(1-R)^4 - 4R^2T^2}}{2R^2T} \right]. \tag{3.7}$$

The computer program IGOR Pro was used to process the data as above and to fit Lorentzian curves to determine the energy positions of the spectral lines.

Chapter 4. Results and Discussion

In this Chapter, the results obtained for the Landau lines of the defects ZnH and Zn^0 in Ge for **B**||<100> are presented and analysed.

4.1. ZnH

The unperturbed transmission spectrum of ZnH in Ge, identified in Figure 3.3 as 'UST 44 hrs', is shown in Figure 4.1 in absorption. The very strong absorption beyond the G line of Zn^0 is due to the D, C, etc., lines of this impurity. The spectral range 65 – 95 cm^{-1} of Figure 4.1. is shown in Figure 4.2, where it is seen that not only is ZnH present but also Al, Ga and P.

A series of spectra of ZnH in Ge at different values of B = |**B**| for **B**||<100> is given in Figures 4.3. and 4.4. for **E**⊥**B** and **E**||**B**, respectively. The group of Zeeman components shown below ~100 cm^{-1} is due to transitions between bound states of ZnH, and are reported in [25]. The lines labelled I_a, I_b and I_c are the main features of the Landau spectrum. Figure 4.5. shows spectra for both polarizations at 4 and 6 T. The shifts of the Landau lines I_a, I_b and I_c from B= 4 T to 6T in 0.25 T steps for both polarizations are shown in Figure 4.6. The Landau line I_a is shown in detail in Figures 4.7. and 4.8. for **E**⊥**B** and **E**||**B**, at 5 and 6 T, while I_b is shown in Figure 4.9 for **E**||**B** at these two fields; this feature does not show any structure for **E**⊥**B**. It can be seen that I_a consists of two components, one a weak, lower energy feature presented as a I_{a1} and a higher energy intense feature labelled I_{a2}. For I_b, the more intense line is the one of lower energy, I_{b1} and weak feature is I_{b2}. In these three figures double Lorenztians have been fitted, simultaneously, to the experimental absorption lines.

Figure 4.10. gives the dependence of the energies of the Landau lines I_a, I_b and I_c on B. Also shown are the data for boron in Ge for **B**||<100> [12] and the result of Hensel and Suzuki for light hole Landau levels [19] adapted to match the ionisation energy of boron [12]. The ZnH data are fitted by straight lines for both polarizations; these are the full lines in Figure 4.10. The boron data are fitted by the straight dashed lines. It should be noted that for boron the lines also contain several components, only

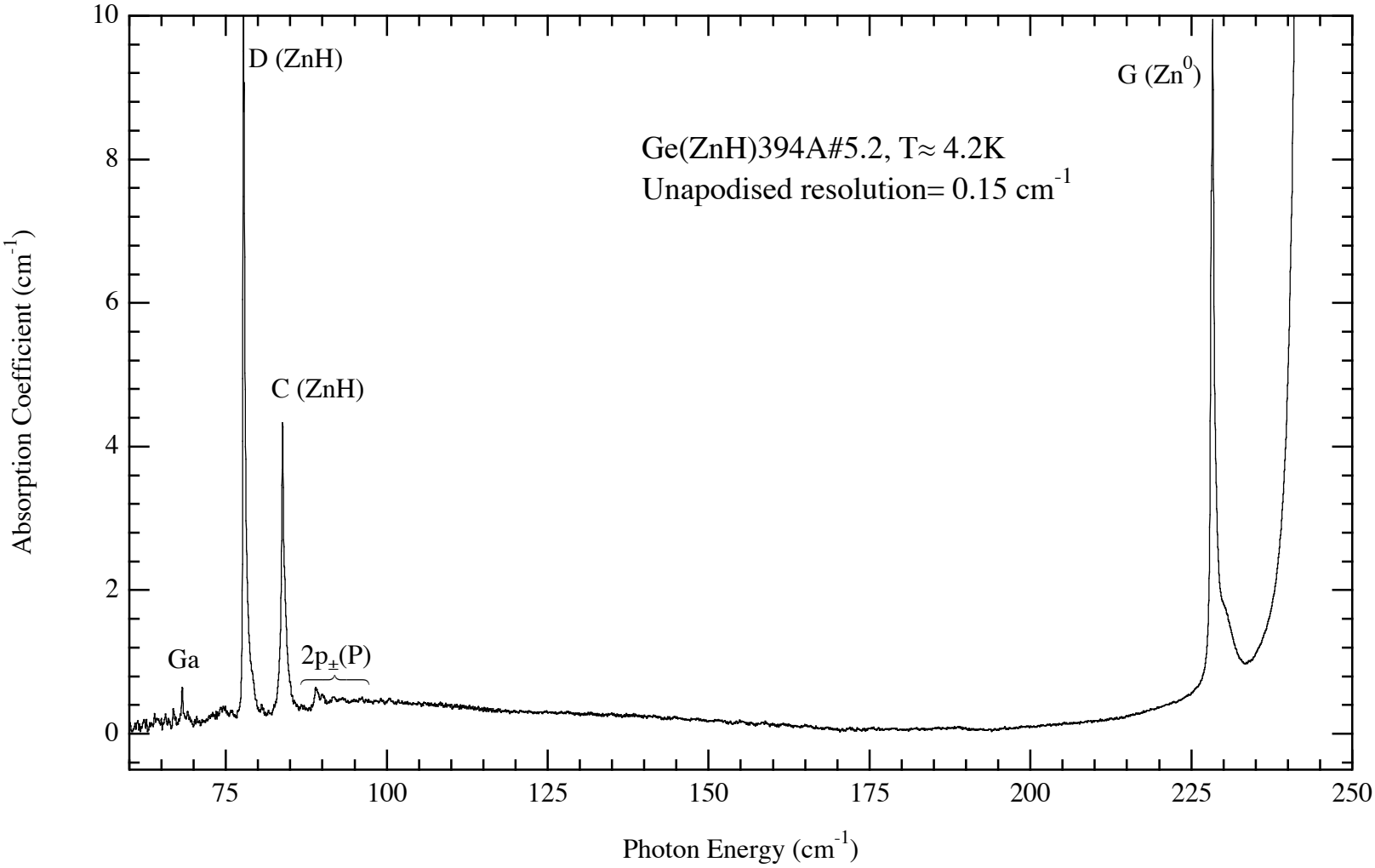

Fig. 4.1. Unperturbed spectrum of the sample used for studying the Landau lines of axial defect ZnH in Ge for **B**||<100>.

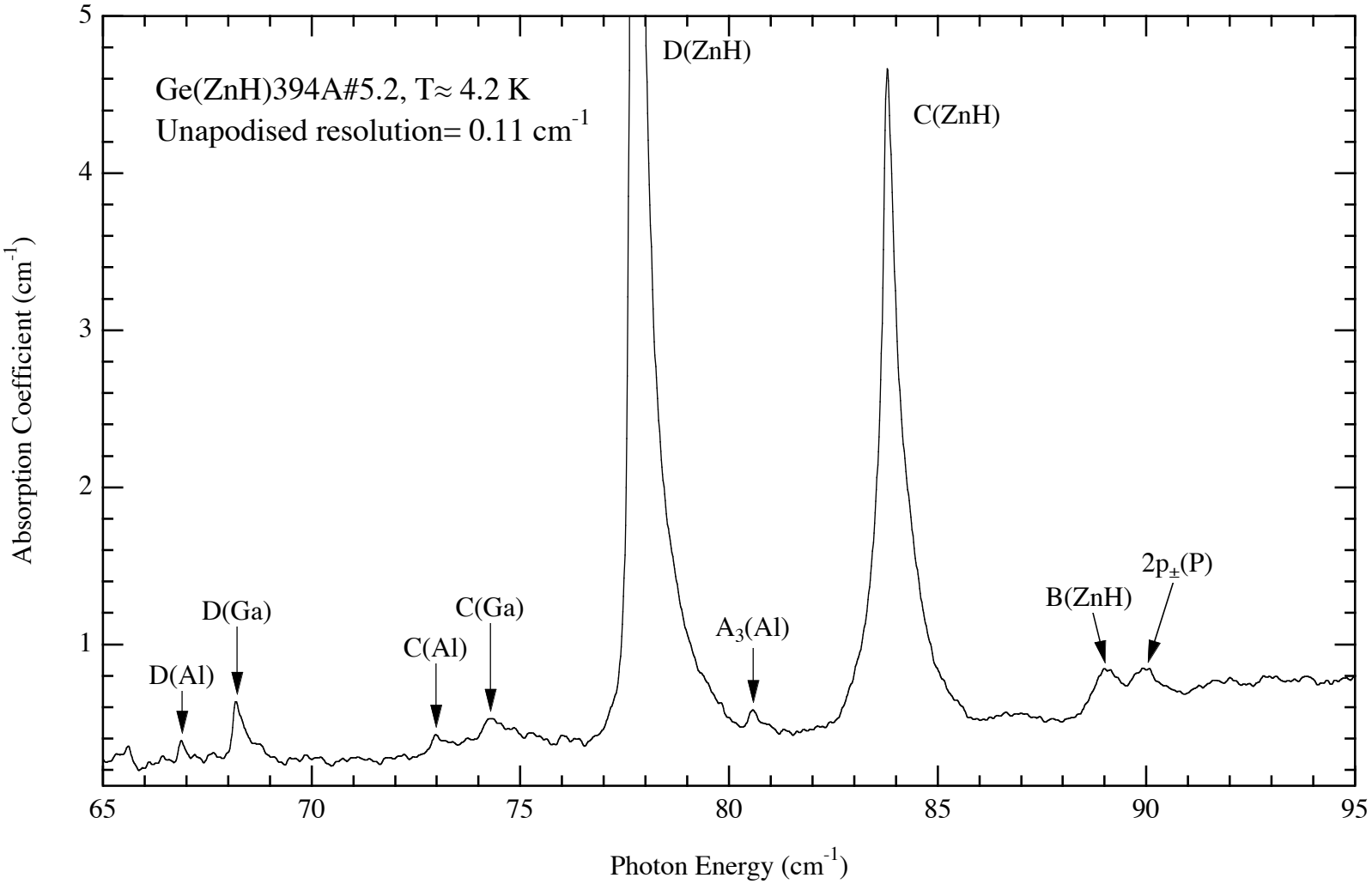

Fig. 4.2. Unperturbed spectrum of the sample of Figure 4.1 in the range of 65 - 95 cm^{-1}.

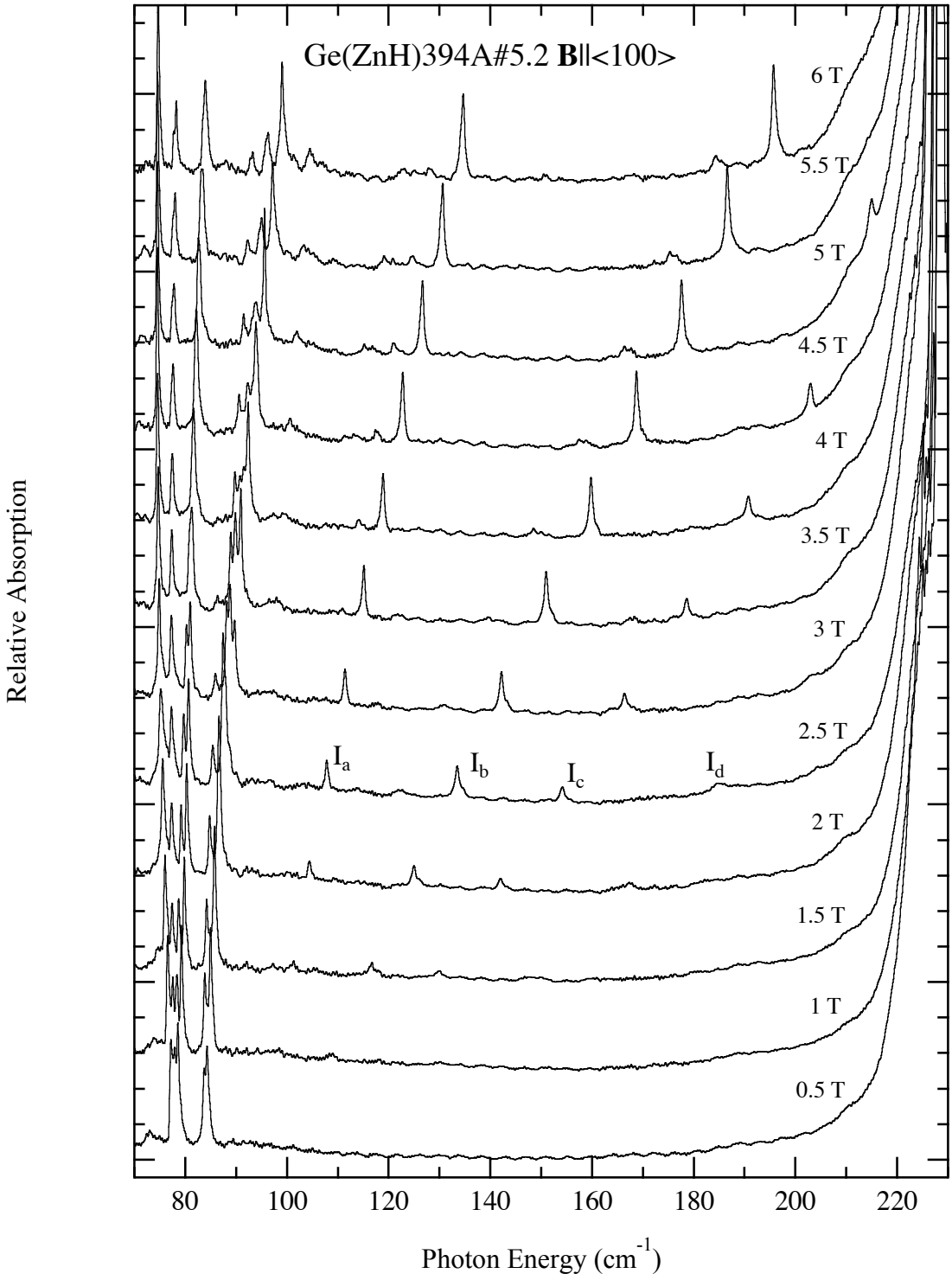

Fig. 4.3. Set of spectra of ZnH in Ge for **E**⊥**B**.
T≈ 4.5 K. Unapodised resolution = 0.37 cm^{-1}.

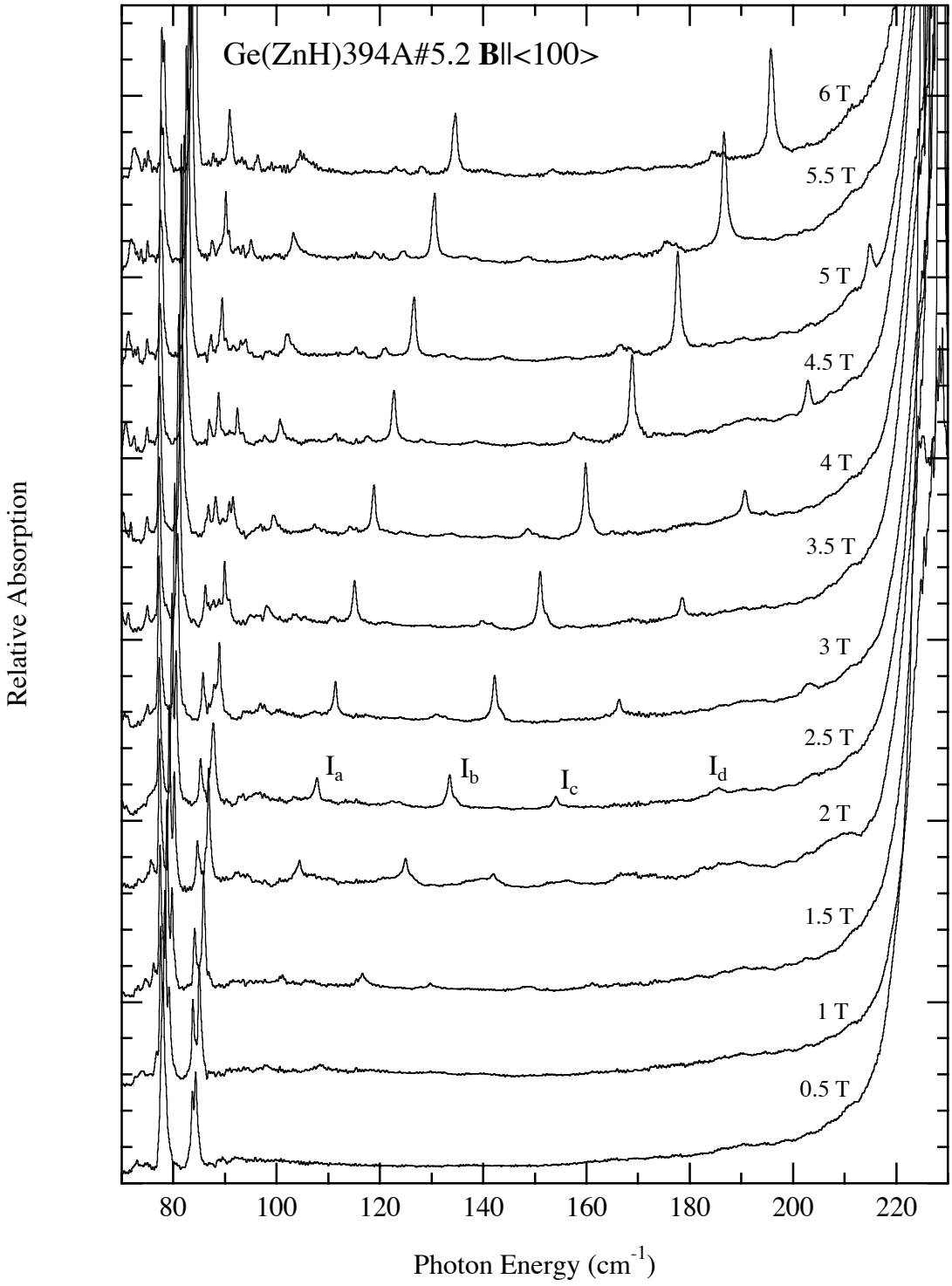

Fig. 4.4. Set of spectra for ZnH in Ge for **E**||**B**.
T≈ 4.5 K. Unapodised resolution = 0.37 cm^{-1}.

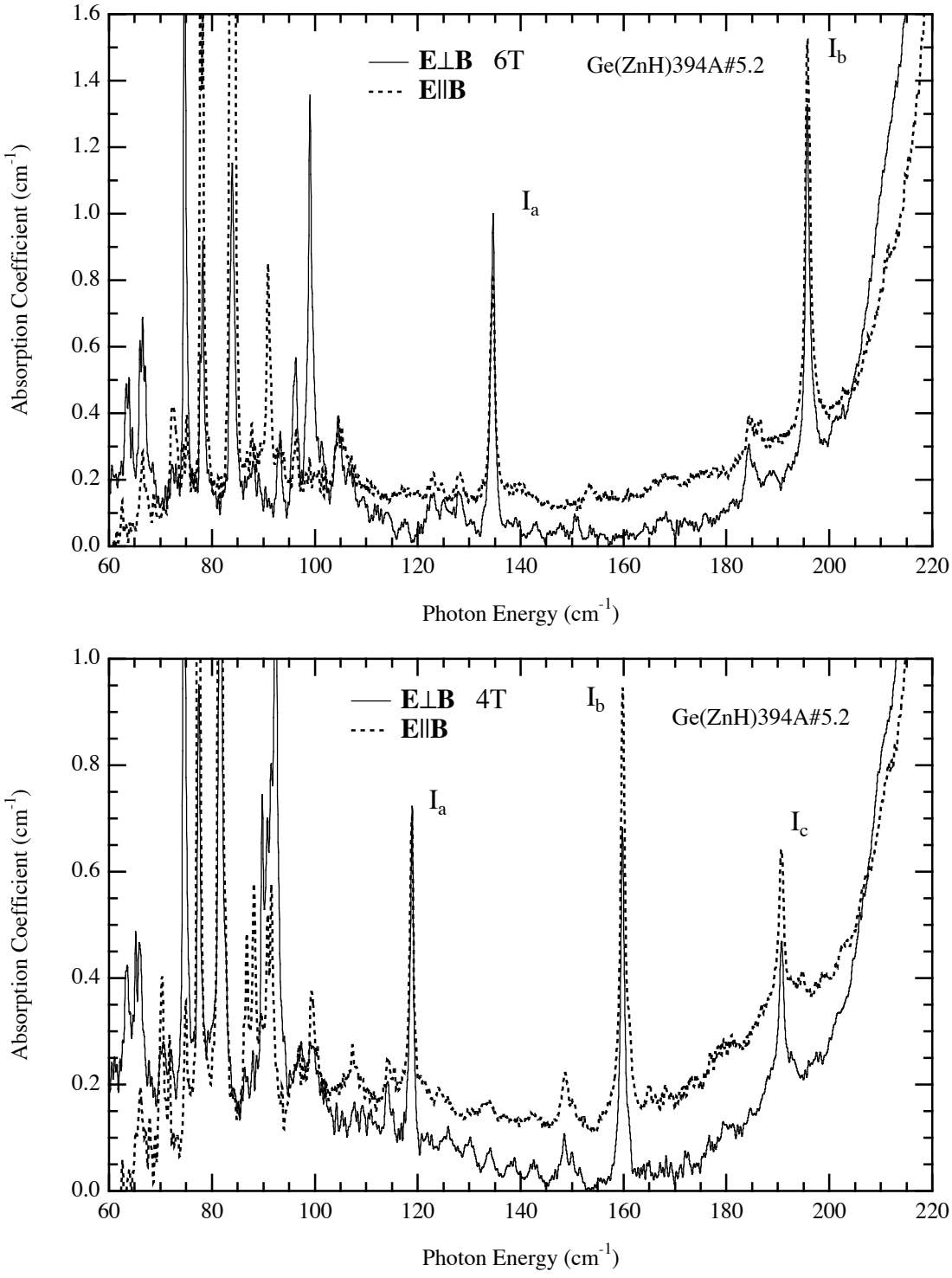

Fig. 4.5. Landau spectra of Ge(ZnH) **B**||<100> for both polarizations. Dashed spectra are for **E**||**B**. Full lines are for **E**⊥**B**. T≈ 4.5 K. Unapodised resolution = 0.37 cm^{-1}.

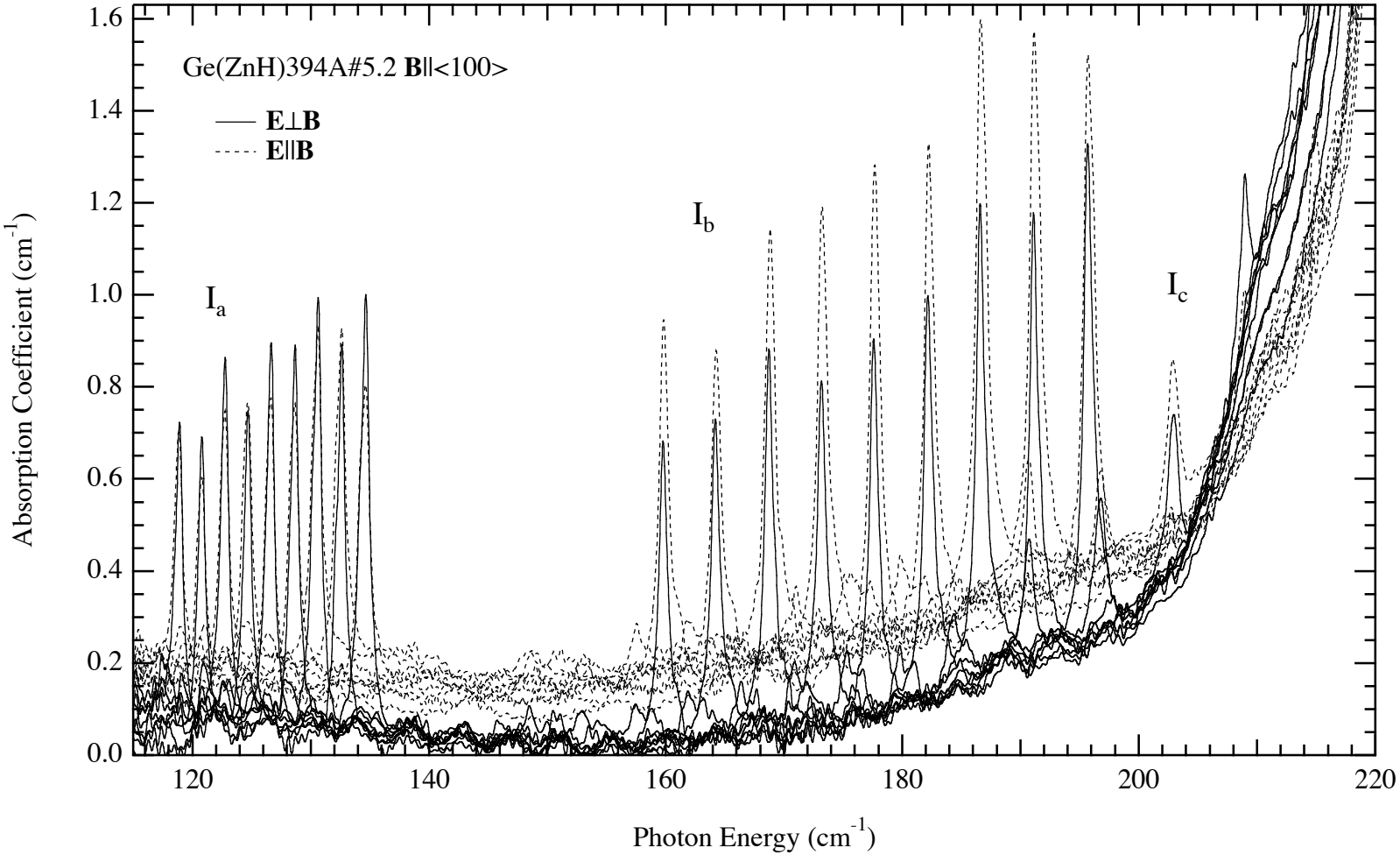

Fig. 4.6. Series of Landau spectra of Ge(ZnH) for **B**||<100> for both polarizations. Magnetic field strength from 4 T to 6 T. Full lines show **E**⊥**B** and dashed lines show **E**||**B**. Unapodised resolution = 0.37 cm^{-1}.

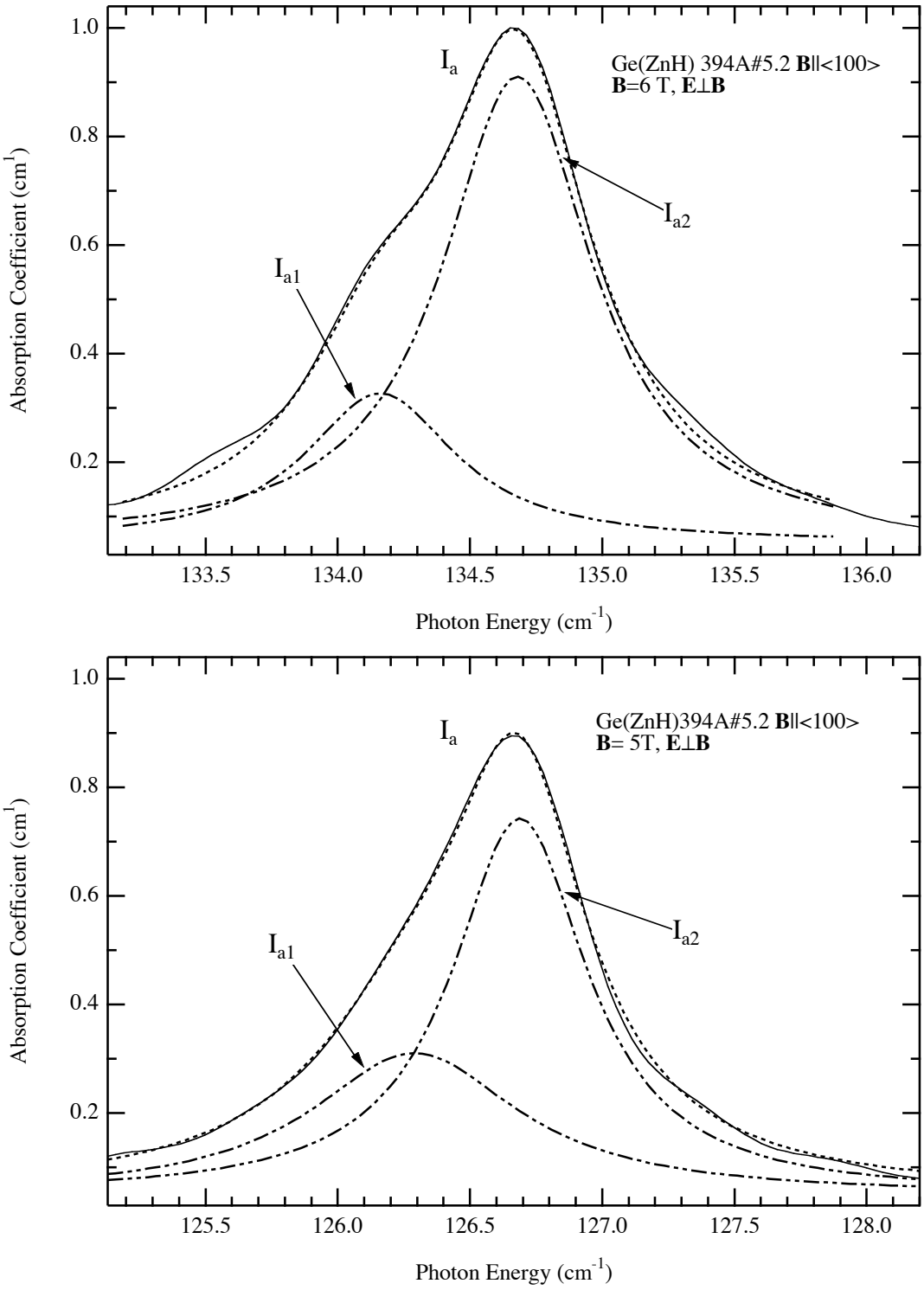

Fig. 4.7. Two Lorentzian fits to Landau line I_a of Ge(ZnH), with magnetic field of 5 and 6 T for **E**⊥**B**. T≈ 4.5 K. Unapodised resolution = 0.37 cm^{-1}.

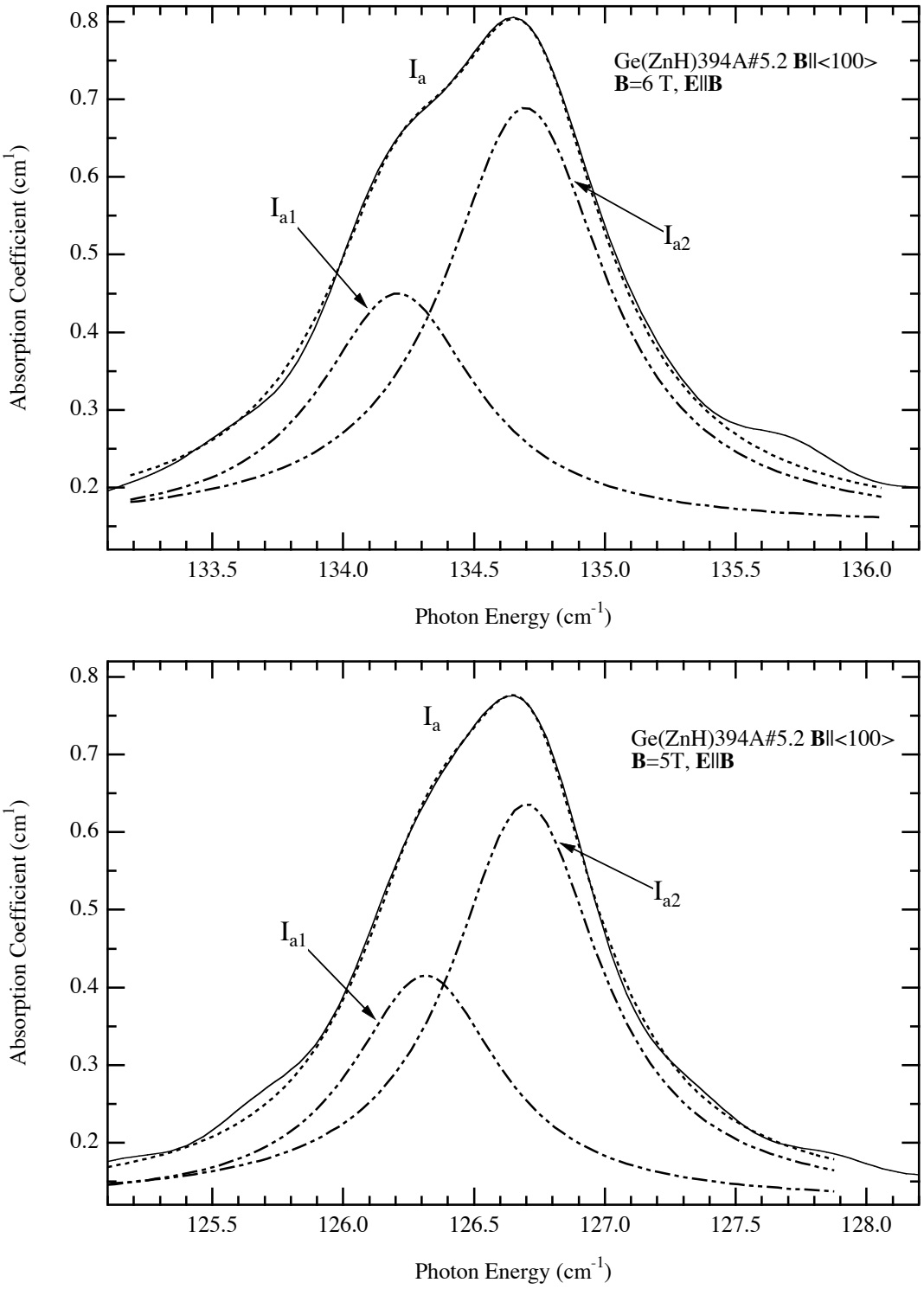

Fig. 4.8. Two Lorentzian fits to Landau line I_a of Ge(ZnH), with magnetic field of 5 and 6 T for **E**||**B**. T≈ 4.5 K. Unapodised resolution = 0.37 cm^{-1}.

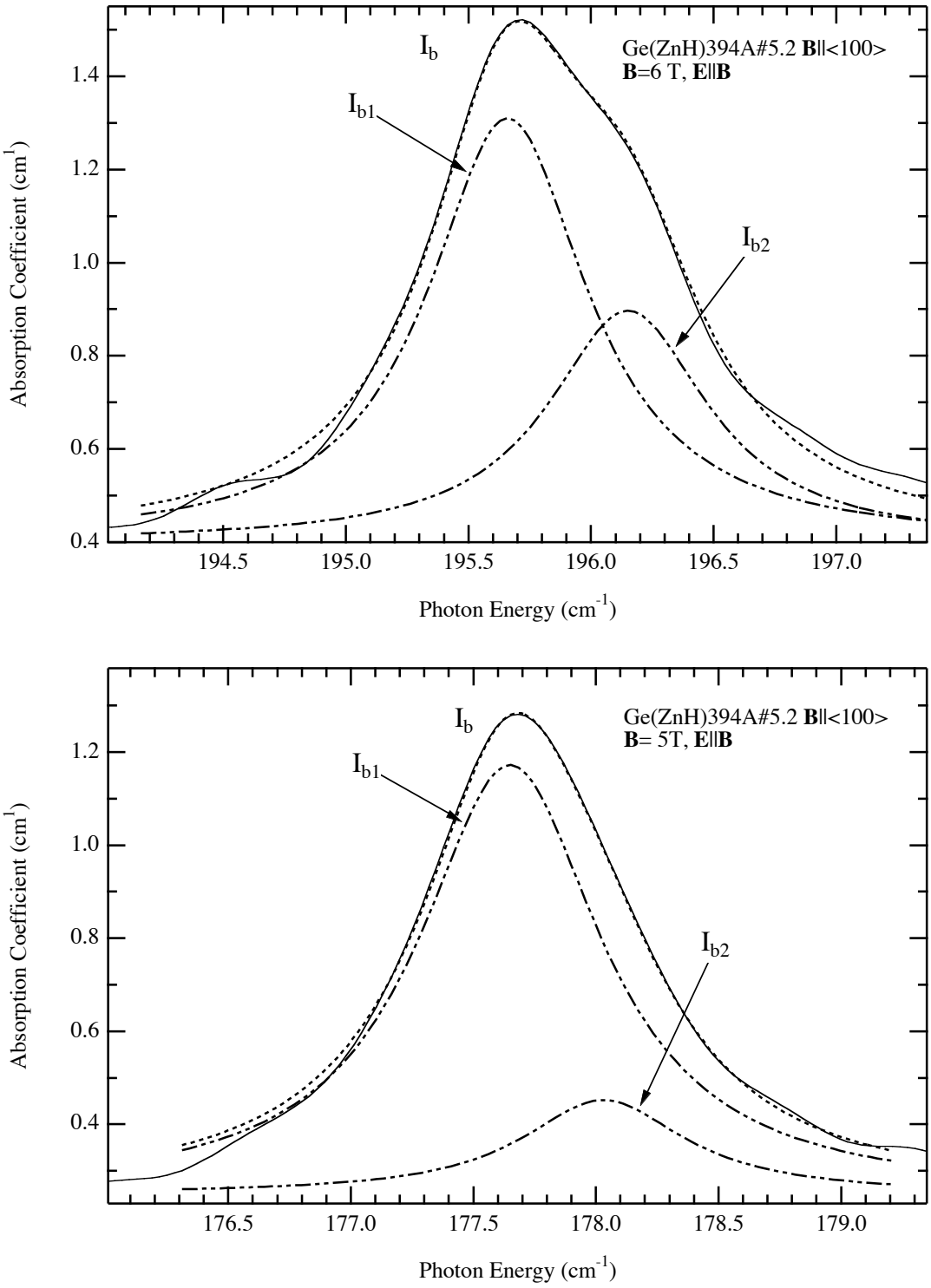

Fig. 4.9. Two Lorentzian fits to Landau line I_b of Ge(ZnH), with magnetic field of 5 and 6 T for **E**||**B**. T≈ 4.5 K. Unapodised resolution = 0.37 cm^{-1}.

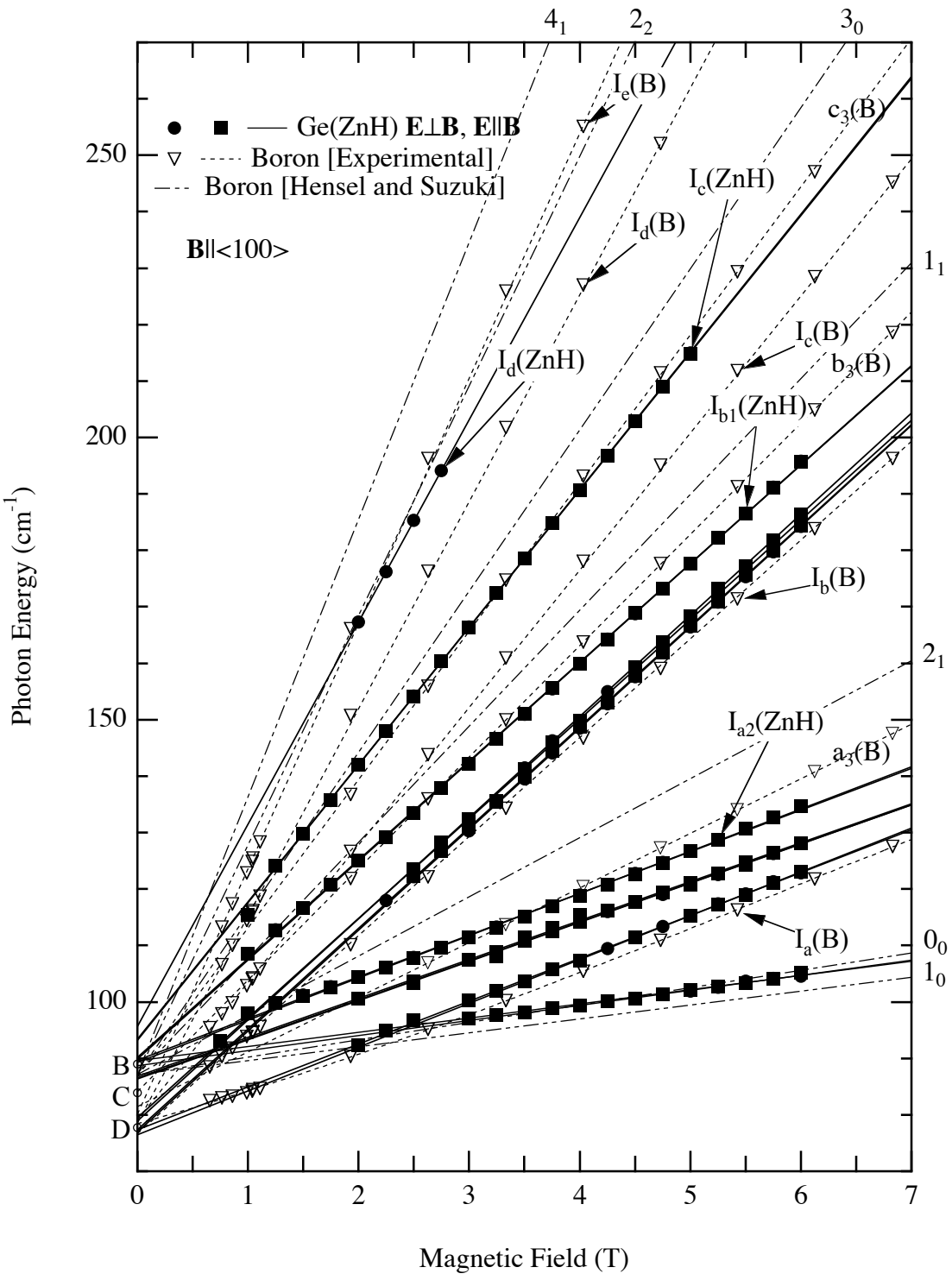

Fig. 4.10. Field dependence of the energies of the Landau lines of ZnH in Ge for both polarizations and boron in Ge with **E**⊥**B** for **B**∥<100>. Also shown are the results of Hensel and Suzuki for light hole Landau levels adapted to boron in Ge.

one is given in Figure 4.10. splittings of these have shown to be due to the Zeeman splitting of the ground state [12] of this impurity (see Figure 2.3).

The labelling of ZnH Landau lines is based on the correlation between the field dependence of the ZnH and boron Landau data. For example, feature labelled I_a(ZnH) has essentially the same energy dependence on B as the boron Landau line I_a(B). The displacement in energy of I_a(ZnH) relative to I_a(B) at a given field is just the difference in the binding energies of these two, *viz*., ~13.6 cm^{-1}. The same results are obtained for I_b(ZnH), I_c(ZnH) and I_d(ZnH). These data are compared with the boron data in Table 4.1; only the prominent lines are used. Similar correlations were obtained between ZnH and boron in Ge for **B**||<111> [13].

Table. 4.1. Field dependence of Landau transitions of ZnH and boron in Ge. B||<100>.

Transition	Field Dependence of Landau lines of ZnH (cm^{-1}/T)	Field Dependence of Landau lines of Boron (cm^{-1}/T)
I_a	7.38 ± 0.07	7.6 ± 0.4
I_b	17.5 ± 0.06	17.6 ± 0.4
I_c	24.33 ± 0.03	24.2 ± 0.4
I_d	35.81 ± 0.16	36.2 ± 0.5

As already discussed, and shown in Figures 4.7 – 4.10, the Landau lines I_a and I_b of ZnH are split. The splitting of I_a(ZnH) as a function of B is shown in Figure 4.11. As this splitting is small, it can be observed only at the higher magnetic fields since its two components have half widths of ~0.7 cm^{-1}. This splitting has not been seen for the higher energy Landau lines I_c(ZnH) and I_d(ZnH), possibly because they are weak and have moved into the region of high absorption for the fields at which the splitting would be large enough to be observed. In Figure 4.12, the splittings of I_a and I_b are compared with the Zeeman splitting of the ground state of ZnH [25] which is given by the quadratic fit to the ZnH data. From this, taking into account the experimental error, it is apparent that the origin of the splitting of I_a(ZnH) and I_b(ZnH) is due to the Zeeman splitting of the ground state of ZnH, noting also that the selection rules for ZnH

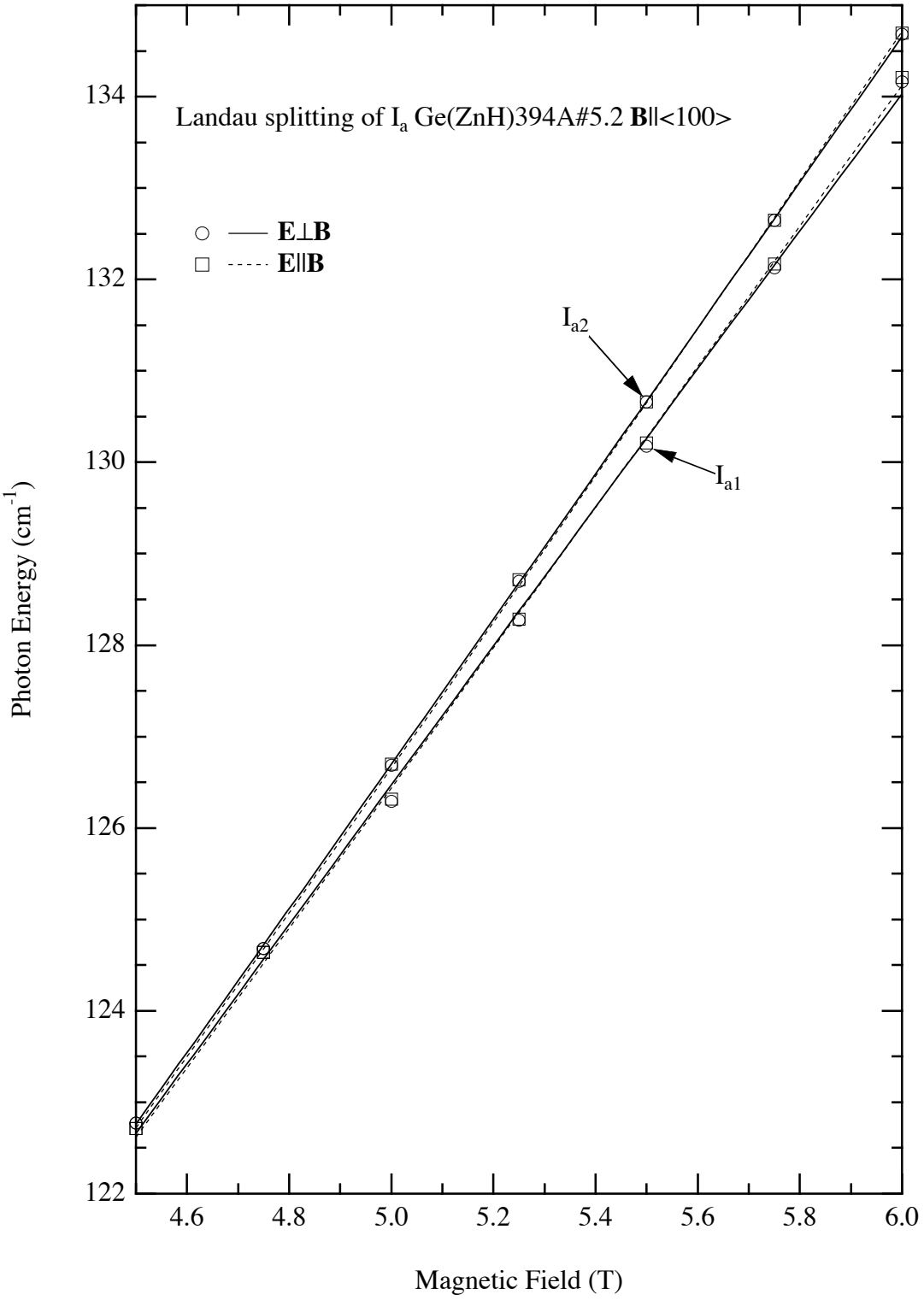

Fig. 4.11. Landau splitting of I_a(ZnH) **B**||<100> for both polarizations.

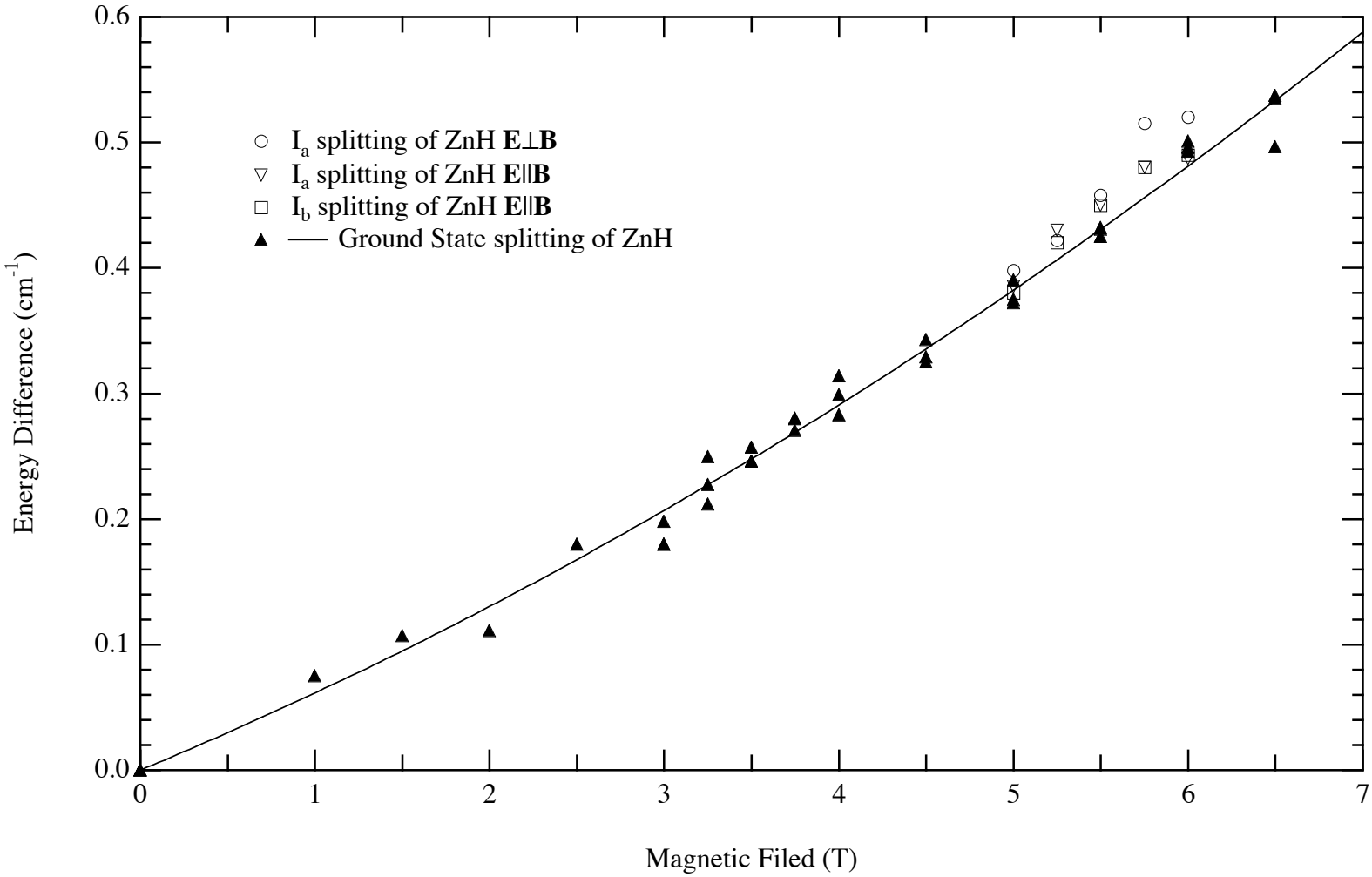

Fig. 4.12. Comparison of the splittings of Landau I lines with the those of ground state of ZnH **B**||<100>. The quadratic fit to the data points of the ground state splitting of ZnH.

BII<100> mentioned in Chapter 2 permit transitions from both Zeeman ground states to any excited state.

4.2 Neutral Zinc (Zn◦)

The unperturbed absorption spectrum of the Ge sample used to observe the Landau lines of Zn◦ in Ge with BII<100> is shown in Figure 4.13; this was obtained using the Bomem spectrometer. The spectrum in the range from 65 to 95cm^{-1} is given in Figure 4.14. This is the sample whose optical faces had been polished, etched and then repolished but not subjected to any UST. At the resolution used for this measurement there no observable splitting of the sharp acceptor lines indicating that any remaining surface damage is small [32]. It can be seen that this sample not only contains Zn◦ but also Ga, ZnH, P and Zn^{-}.

A series of spectra with B||I<100> for different values of B is given in Figures 4.15 and 4.16 for E ⊥ and EIIB, respectively. The group of Zeeman components at energies below ~280cm^{-1} are due to transitions between bound states and has been reported elsewhere [29]. The two strong, broad features centred at ~350cm^{-1} are the main lattice vibration bands of Ge; the Landau lines can not be followed as they pass through these bands. The main Landau lines are labelled I_a to I_i. Figure 4.17 shows the spectra for both polarizations of 6 T on a larger scale with more detailed labelling of the Landau lines. Each Landau line has one component for EIIB lying between two components for E ⊥ B. Figure 4.18 gives the dependence of the energies of the Landau spectral features on B; these data are combined with those of boron in Ge for BII<100> and the result of Hensel and Suzuki for light hold Landau levels. As was the case for ZnH, the correlation obtained between the Zn◦ and boron Landau data justifies the labelling of the features of Zn◦. In Table 4.2, the field dependence of each Landau line of Zn◦ is different to that of, for example, line I_a of boron in that the splittings at a given B of the Landau lines of Zn◦ are more than twice those of boron. As already stated above, the splittings of the Landau lines of boron have been shown to be due to the Zeeman splitting of its fourfold degenerate ground state [12].

Please see print copy for Table 4.2

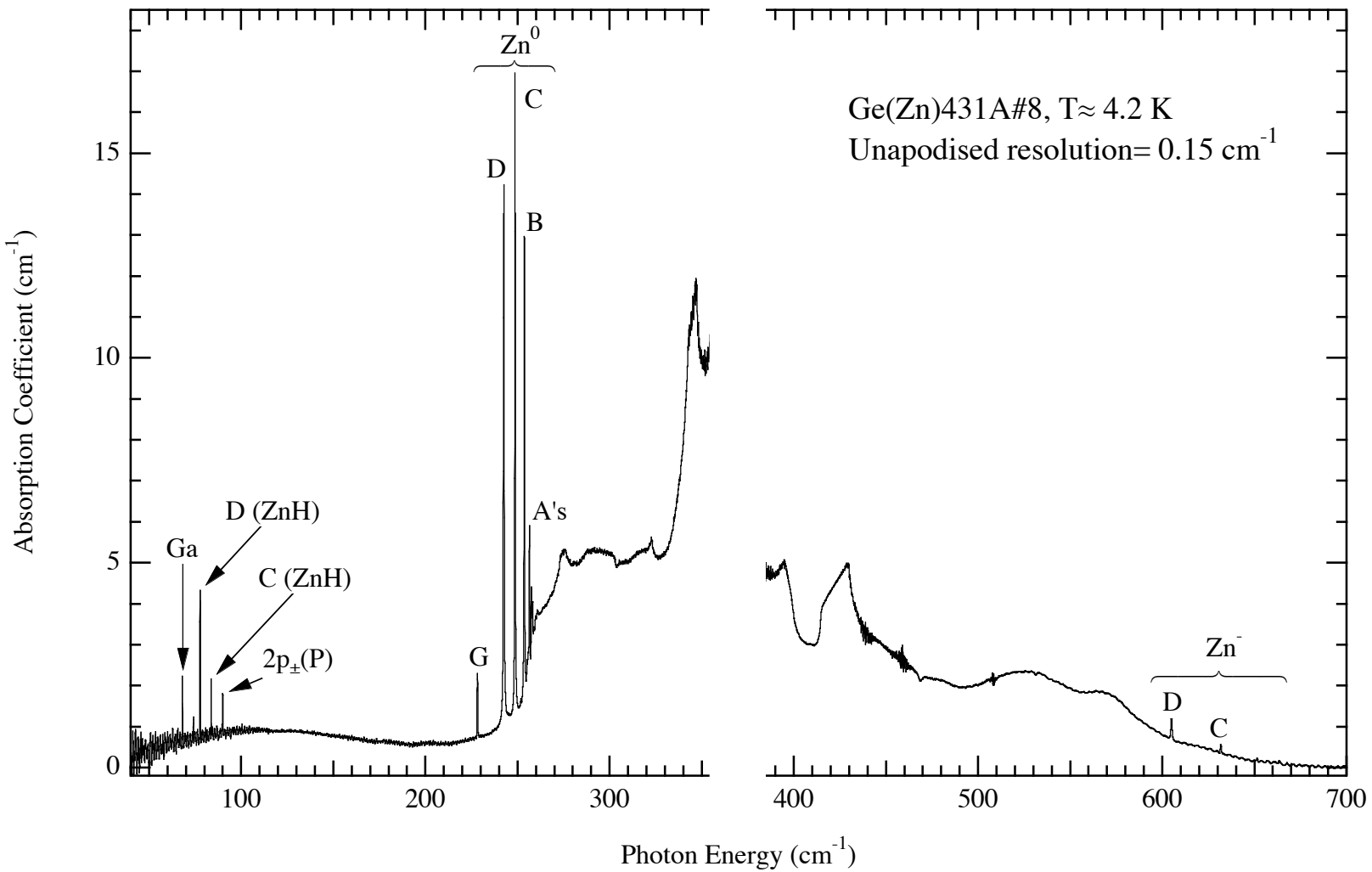

Fig. 4.13. Unperturbed spectrum of the sample used for studying the Landau lines of neutral zinc in Ge for **B**||<100>.

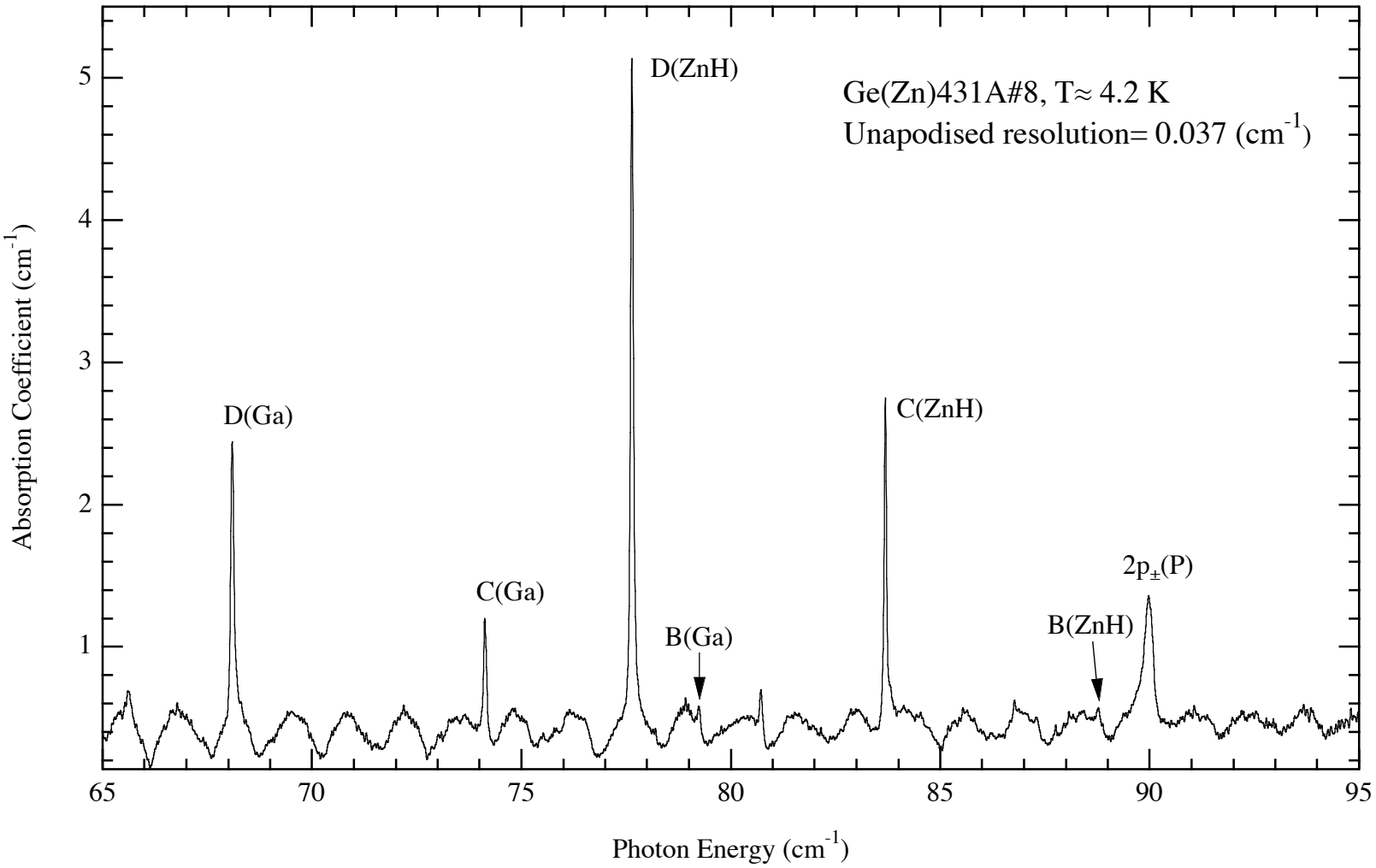

Fig. 4.14. Unperturbed spectrum of the sample of Figure 4.13 in the range of 65 - 95 cm^{-1}.

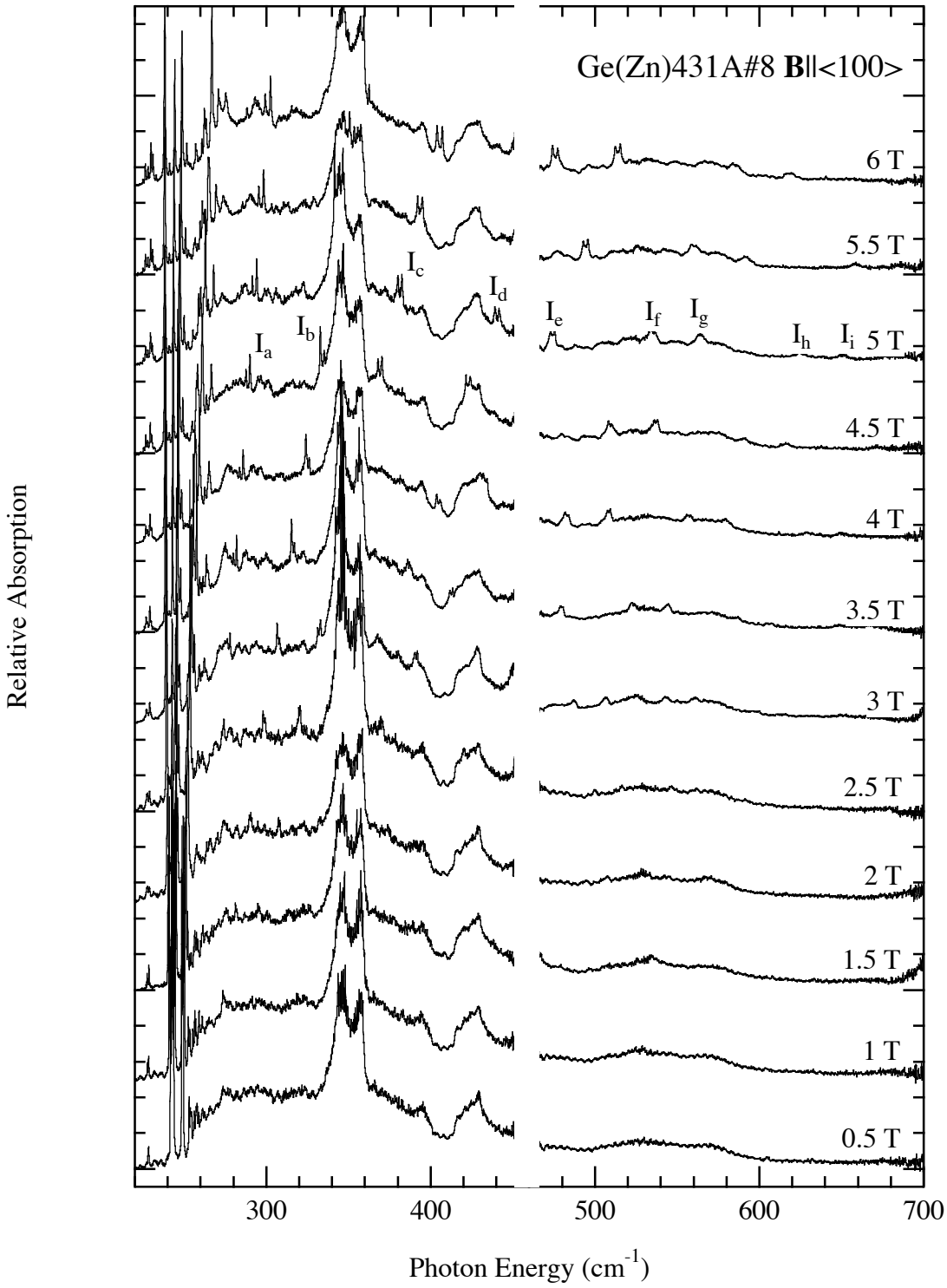

Fig. 4.15. Set of spectra of neutral Zn in Ge for **E**⊥**B**.
T≈ 2.5 K. Unapodised resolution = 0.37 cm^{-1}.

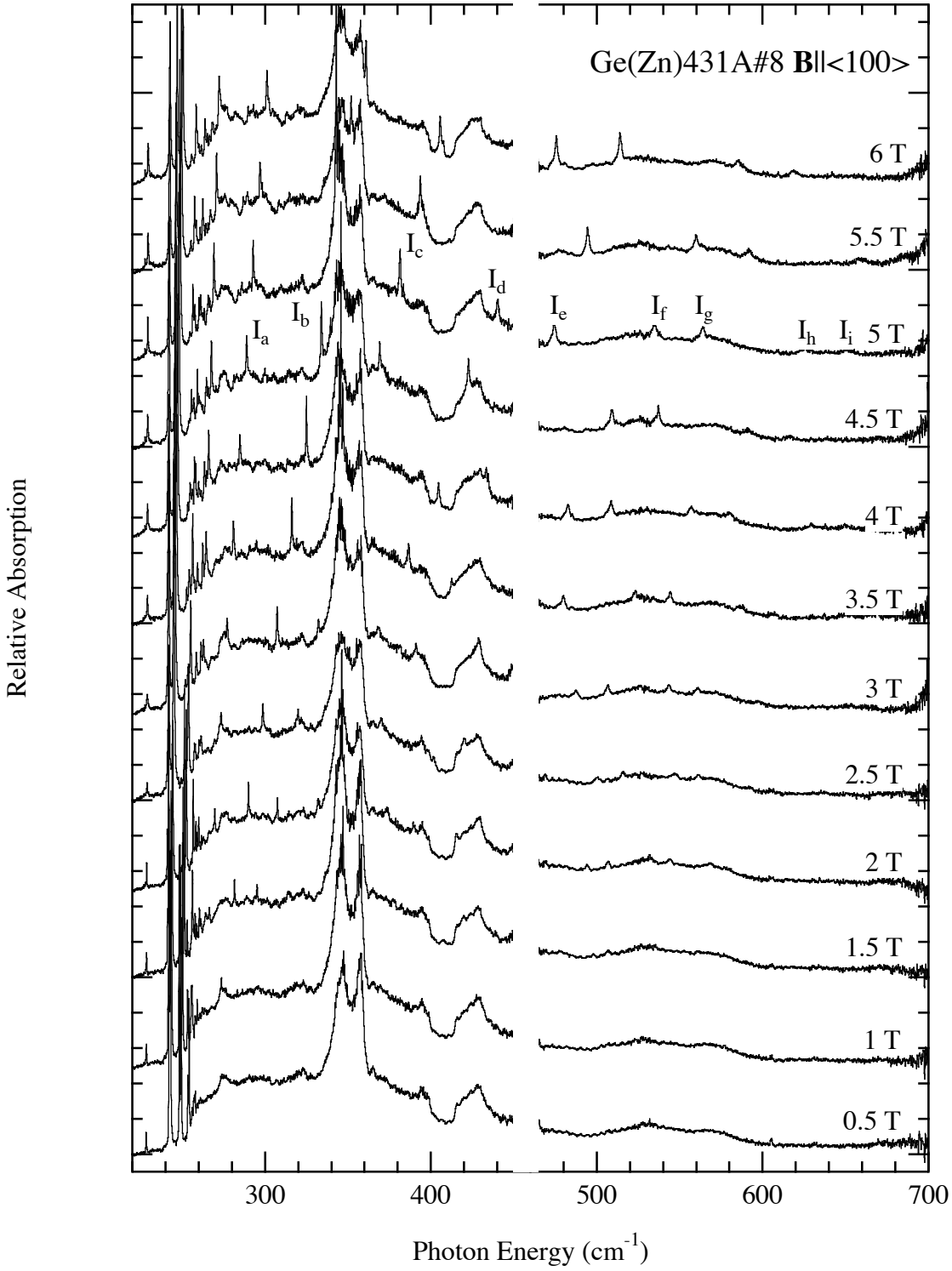

Fig. 4.16. Set of spectra of neutral Zn in Ge for **E**||**B**.
T≈ 2.5 K. Unapodised resolution = 0.37 cm^{-1}.

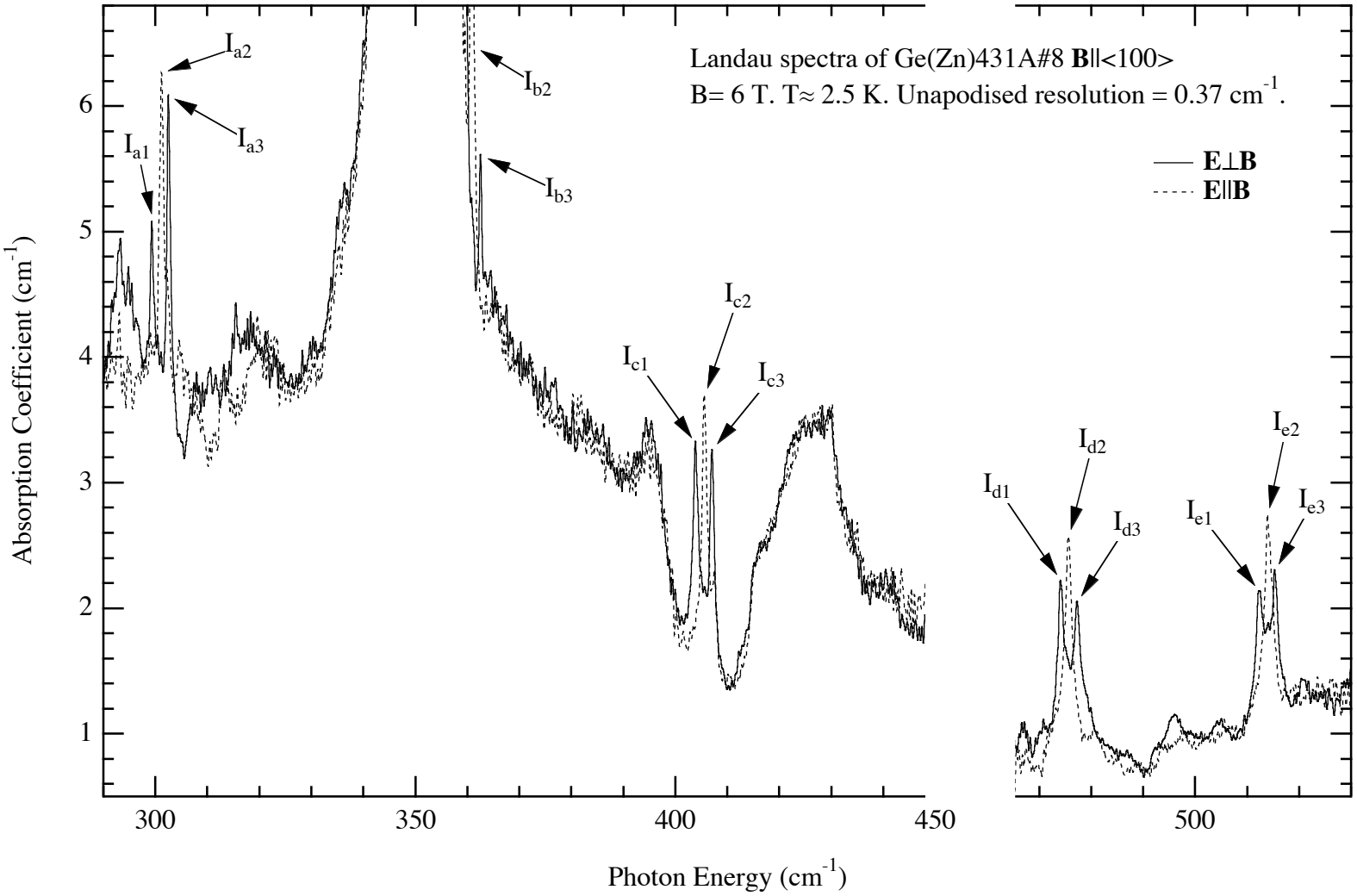

Fig. 4.17. Landau spectra of neutral Zn in Ge for **B**||<100> at B= 6 T for both polarizations.

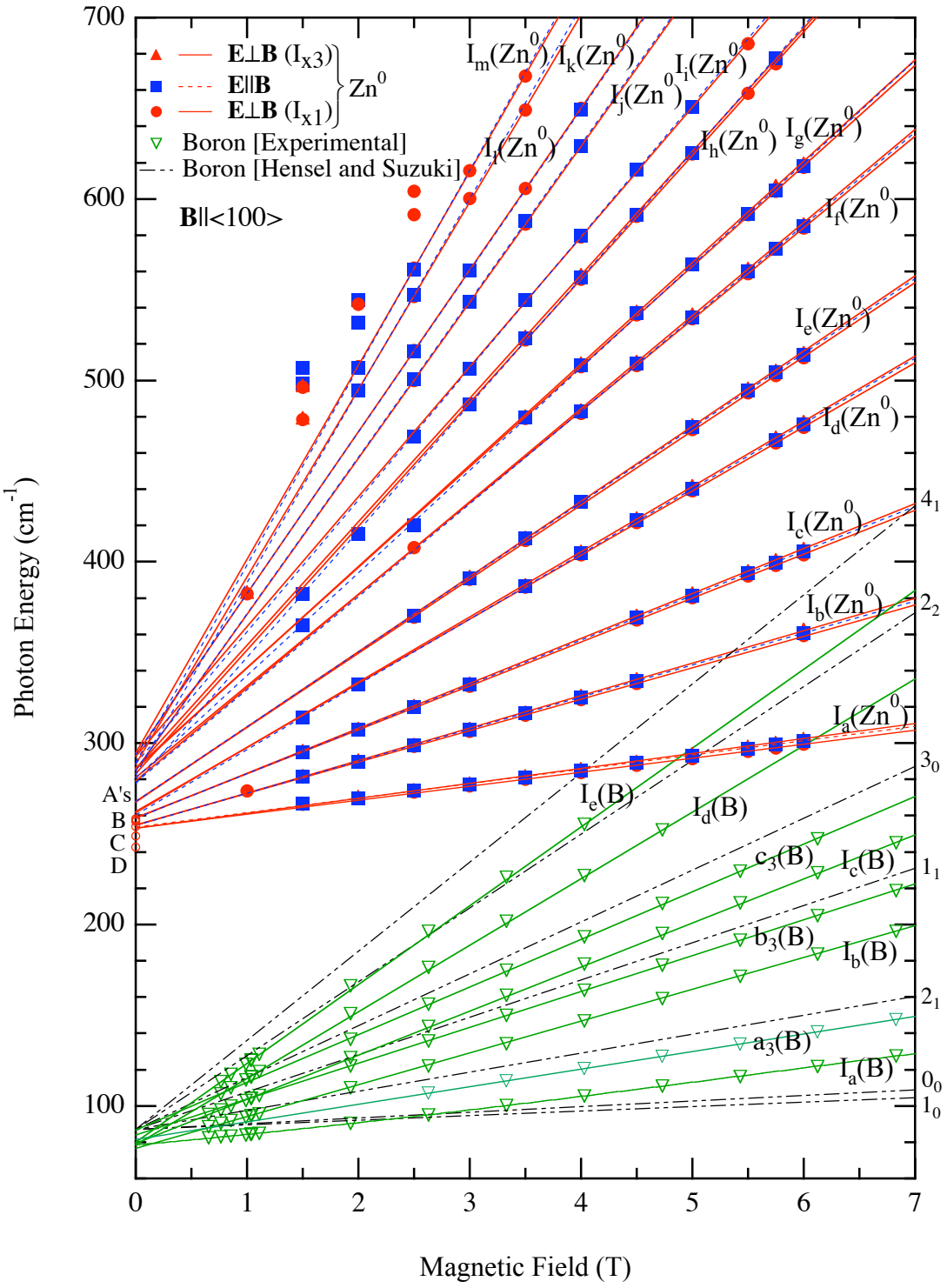

Fig. 4.18. Field dependence of the energies of the Landau lines of Zn^0 in Ge for both polarizations (See Fig. 4.17 for I_x's) and boron in Ge with **E⊥B** for **B**||<100>. Also shown are the results of Hensel and Suzuki for light hole Landau levels adapted to boron.

The dependence on B of the splittings of the components of the Landau lines of Zn^o is given in Figures 4.19. The upper set of data points is the average of the spacings of I_{x3} and I_{x1}, where a=a, b, c, d, e (see Fig 4.17). The lower set of data points is the average of the spacings of I_{x3} and of I_{x2} and also of I_{x2} and of I_{x1}. The straight lines in this figures are not fits to the data but are the Zeeman splittings of the ground state of Zn^- as obtained from Zeeman measurements on the D line of this singly ionised impurity [31] (Figure 4.13 shows this feature at ~605 cm^{-1}). Thus, it is clear that structure of the I lines of Zn^o is due to the four different Zeeman ***excited states*** of Zn^o. As discussed in Chapter 2, there are four sets of Landau excited states for Zn^o; these are seen in Figure 2.4 each depending upon which Coulomb-related final state the excited hole occupies. Also shown in Figure 2.4 are the three allowed transitions for each of these cases. The experimental data shown in Figure 4.17 reveal three transitions for all of the I lines as permitted by the selection rules. However, in each case the parallel component falls between the two perpendicular components. Only two of the cases in Figure 2.4 allow this disposition. This implies that a Landau state involved in a given excitation is either of Γ^-_5 or Γ^-_6 symmetry. In the work on boron [12] for BII<100>, from the selection rules it was deduced unambiguously that the final Landau state for I_b 'belonged' was 1_b. Correlation between the Landau levels shown in Figure 2.2 and their symmetries is given in Eqns 2.12; it is seen that 1_1 has Γ^+_6 symmetry. It was thus assumed that, except for the parity, the Coulomb state at the bottom of each Landau sub-band has the same symmetry as that of the associated sub-band. Since I_a and I_c, for example, were deduced to be transitions associated with the Landau levels 2_1 and 3_0, respectively, then, according to Eqns 2.12, their symmetries should be Γ^-_5 and Γ^-_8, respectively. Of these, the former agrees with the present results but the latter does not. The origin of this discrepancy is not clear, however, ti may be simply that the assumed relationship between the symmetry of the Landau impurity states and that of their related Landau sub-bands is not correct.

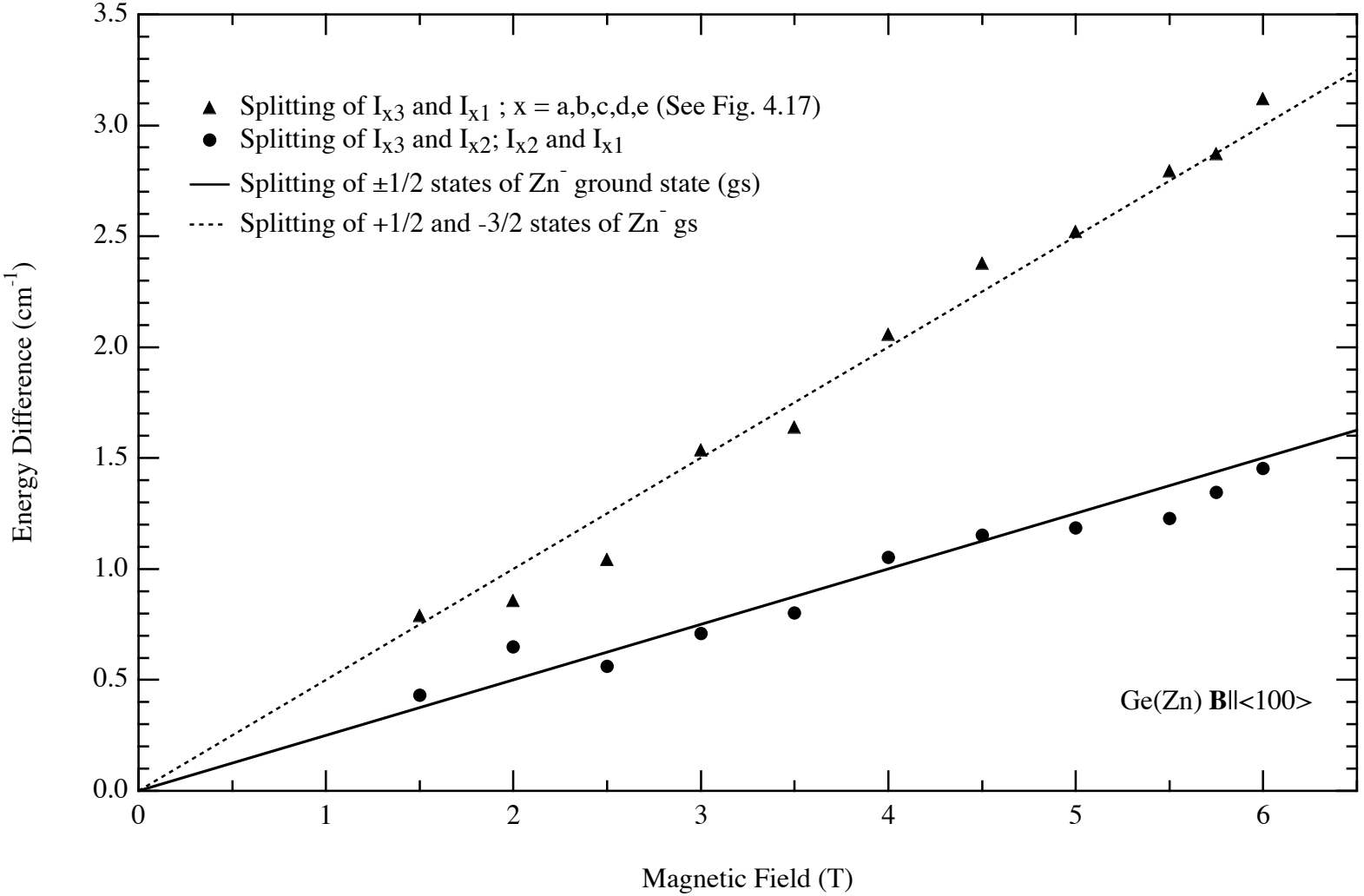

Fig. 4.19. Field dependence of the splitting of the I lines of Zn^0 and the ground state of Zn^- in Ge **B**||<100>.

Chapter 5. Conclusions.

A study has been made of the Coulomb-related Landau excitation lines of the axial defect ZnH and the double acceptor neutral zinc, Zn^0, in germanium; in both cases the magnetic fields were applied along <100> crystallographic directions. The observations involved measurement of their optical absorption spectra. The results obtained have been compared with those for boron in germanium for the same orientation of field and covering a similar range of magnetic field strengths. It has been determined that each of the main features of the spectra from the three acceptors, boron, ZnH and Zn^0, is associated with the same Landau level. This has been deduced from the almost identical field dependence of a given Coulomb-related Landau line in the spectrum of each impurity. The difference between the spectra lies in the fine structure corresponding features exhibit.

Previous detailed studies of this type for boron in germanium demonstrate that any complexity in a given feature is due to the Zeeman splitting of the ground state of boron. Since this state is fourfold degenerate, it separates into four magnetic states whose splittings are known quantitatively as a function of field. These splittings at the fields used are not linear functions of field and are reflected directly in the splittings of the Landau lines of boron. The impurity states related to the Landau sub-bands are Zeeman singlets.

In the case of ZnH, the Zeeman splitting of its ground state is also known as a function of field strength. However, the ground state of this defect is only twofold degenerate with a simpler dependence on field than for boron. As for boron, this splitting is manifested in the Landau lines of ZnH while again the impurity states related to the Landau sub-bands are Zeeman singlets.

For neutral zinc, it is the complexity of the excited states which is revealed in the observed splitting of the Landau lines and not the ground state. The symmetries of the impurity states associated with the related Landau sub-bands have been narrowed from four to two choices for all the observed Landau lines. Some of these are in agreement with those deduced for the case of boron. Why not all agree is of interest and needs to be explored further.

References

[1] W.J. de Haas and P. M. van Alphen, *Proc. Amsterdam Ac.* **33**, 1106 (1930).

[2] L. Shubnikov and W.J. de Haas, *Commun.Phys. Lab. Univ. Leiden* **207**, 210 (1930).

[3] L. Landau, *Z. Physik* **64**, 629 (1930).

[4] D. Shoenberg, *Proc. 9th Int. Conf. On Low Temp. Phys.,* ed. Daunt, Edwards, Milford and Yaqub (Plenum, N. Y., 1965) p. 665.

[5] A. H. Kahn and H. P. R. Frederikse, *Solid State Physics* **9**, ed. F. Seitz and D. Turnball (Acad. Press, 1959).

[6] G. Dresselhaus, A. F. Kip and C. Kittel, *Phys. Rev.* **92**, 827 (1953); *ibid*, **98**, 368 (1955).

[7] R. N. Dexter, H. J. Zeiger and B. Lax, *Phys. Rev.* **104**, 637 (1956).

[8] M. I. Axbel' and E. A. Kaner, *Sov. Phys. JETP* **3**, 772 (1956).

[9] E. Burstein, G. S. Picus, R. F. Wallis and F. Blatt, *J. Phys. Chem. Solids* **8**, 305 (1959); B. Lax, L. M. Roth and S. Zwerdling, *ibid*, 311 (1959).

[10] H. Y. Fan and P. Fisher, *J. Phys. Chem. Solids* **8**, 270 (1959); W. S Boyle, *ibid*, 321 (1959).

[11] P. Fisher and H. Y. Fan, *Phys. Rev. Letters* **2**, 456 (1959).

[12] G. J. Takacs, *PhD Thesis*, University of Wollongong (1999), unpublished, G. J. Takacs and P. Fisher, *phys. stat. sol.(b)* **215**, 143 (1999).

[13] K. Ishida, *Research Report for Fourth Year of B. Sc. at The University of Electro-Communications, Tokyo, Japan (2001) unpublished*; P. Fisher, R. E. M. Vickers and K. Ishida, *phys. stat. sol. (b)* **0**, 683 (2003).

[14] J. M. Luttinger and W. Kohn, *Phys. Rev.* **97**, 869 (1955).

[15] J. M. Luttinger , *Phys. Rev.* **102**, 1030 (1956).

[16] G. H. Wannier, *Phys. Rev.* **52**, 191 (1937).

[17] R. F. Wallis and H. J. Bowlden, *Phys. Rev.* **118**, 456 (1960).

[18] K. Suzuki and J. C. Hensel, *Phys. Rev. B* **9**, 4184 (1974).

[19] J. C. Hensel and K. Suzuki, *Phys. Rev. B* **9**, 4219 (1974).

[20] R. C. Fletcher, W. A. Yager and F. R. Merritt, *Phys. Rev.* **100**, 747 (1955).

[21] G. F. Koster, J. O. Dimmock, R. G. Wheeler and H. Statz, *Properties of the Thirty-Two Point Groups*, (MIT Press, Cambridge, Mass., 1963).

[22] R. F. Wallis and H. J. Bowlden, *J.Phys. Chem.Solids* **7**, 78 (1958).

[23] P. J. Lin-Chung and B. W. Henvis, *Phys. Rev. B* **12**, 630 (1975).

[24] E. E. Haller, G. S. Hubbard and W, L. Hansen, IEEE Trans. Nucl. Sci. NS-**24,** No. 1,48-52 (1977); R. B. McMurray, Jr., N. M. Haegel, J. M. Kahn and E. B. Hailer, Proc. First Intl. Conference on the Spectroscopy of Shallow Centers in Semiconductors SSCS'84 Berkeley, CA, Aug. 2-3, 1984, E E. Haller, K. K. Bajaj and A. K. Ramdas, eds., Solid State Comm. **53**, 1137 (1985); R. E. McMurray, Jr., N. M. Haegel, J. M. Kahn and E. E. Haller, Solid State Comm. **61**, No. 1, 27-32 (1987); J. M. Kahn, Robert E. McMurray, Jr., E. E. Haller and L. M. Falicov, *Phys. Rev. B* **36**, 8001 (1987).

[25] P. C Jobe Prabakar, R. E. M. Vickers and P. Fisher, *Solid State Commun.* **107**, 85 (1998); *ibid*, *phys. stat. sol. (b)* **210**, 283 (1998). See also Jobe Prabakar Chelliah, PhD Thesis, University of Wollongong (2000). Unpublished.

[26] A. Baldereschi and N. O. Lipari, *Phys. Rev. B* **8**, 2697 (1973); *idid* **9**, 1525 (1974).

[27] R. A. Chapman, W. G. Hutchinson and T. L. Estle, *Phys. Rev. Lett.* **17**, 132 (1966).

[28] M. L. W. Thewalt, B. P. Clayman and D. Labrie, *Phys. Rev. B* ***3*2**, 2663 (1985); D. Labrie, I. J. Booth, M. L. W. Thewalt and E. E. Haller, *Phys. Rev. B* ***3*8**, 5504-10 (1988); D. Labrie, I. J. Booth, M. L. W. Thewalt and E. E. Haller, Phys. Rev. B **38**, 5504-10 (1988); H. Nakata, E. Otsuka and E. E. Haller, Solid State Comm. **80**, 387-90 (1991).

[29] D. S. Ryan, P. Fisher and C. A. Freeth, *Proc. 22nd Int. Conf. Phys. Semiconds., 1994.* Ed. D. J. Lockwood (World Scientific Publ. Co., Singapore, 1997) p. 2375; R. E. M. Vickers, P. Fisher and C. A. Freeth, *phys. stat. sol. (b)* **210**, 839 (1998).

[30] F. S. Ham and C. H. Leung, *Phys. Rev. Lett.* **71**, 3186 (1993); *ibid*., *Solid State Comm.* **93**, 375 (1995).

[31] P. Fisher, C. A. Freeth and R. E. M. Vickers, *phys. stat. sol. (b)* **210**, 827 (1998).

[32] P. Fisher and R. E. M. Vickers, *Appl. Phys. Lett.* **79**, 3458 (2001).